



# Antisense oligonucleotide therapy rescues disturbed brain rhythms and sleep in juvenile and adult mouse models of Angelman syndrome

Dongwon Lee<sup>1,2†</sup>, Wu Chen<sup>1,2\*†</sup>, Heet Naresh Kaku<sup>1,2†</sup>, Xinming Zhuo<sup>3‡</sup>, Eugene S Chao<sup>1,2</sup>, Armand Soriano<sup>4</sup>, Allen Kuncheria<sup>1</sup>, Stephanie Flores<sup>1</sup>, Joo Hyun Kim<sup>1,2</sup>, Armando Rivera<sup>1,2</sup>, Frank Rigo<sup>4</sup>, Paymaan Jafar-nejad<sup>4</sup>, Arthur L Beaudet<sup>3§</sup>, Matthew S Caudill<sup>1,5</sup>, Mingshan Xue<sup>1,2,3\*</sup>

<sup>1</sup>Department of Neuroscience, Baylor College of Medicine, Houston, United States;

<sup>2</sup>The Cain Foundation Laboratories, Jan and Dan Duncan Neurological Research Institute at Texas Children's Hospital, Houston, United States; <sup>3</sup>Department of Molecular and Human Genetics, Baylor College of Medicine, Houston, United States;

<sup>4</sup>Ionis Pharmaceuticals, Carlsbad, United States; <sup>5</sup>Jan and Dan Duncan Neurological Research Institute at Texas Children's Hospital, Houston, United States

\*For correspondence:

wu.chen@bcm.edu (WC);  
mxue@bcm.edu (MX)

†These authors contributed equally to this work

Present address: <sup>‡</sup>CLIA Laboratory, The Jackson Laboratory for Genomic Medicine, Farmington, United States; <sup>§</sup>Luna Genetics, Houston, United States

Competing interest: See page 23

Funding: See page 23

Preprinted: 19 June 2022

Received: 15 July 2022

Accepted: 30 December 2022

Published: 03 January 2023

Reviewing Editor: Samuel Pleasure, University of California, San Francisco, United States

© Copyright Lee, Chen, Kaku et al. This article is distributed under the terms of the [Creative Commons Attribution License](#), which permits unrestricted use and redistribution provided that the original author and source are credited.

**Abstract** UBE3A encodes ubiquitin protein ligase E3A, and in neurons its expression from the paternal allele is repressed by the *UBE3A* antisense transcript (*UBE3A-ATS*). This leaves neurons susceptible to loss-of-function of maternal *UBE3A*. Indeed, Angelman syndrome, a severe neurodevelopmental disorder, is caused by maternal *UBE3A* deficiency. A promising therapeutic approach to treating Angelman syndrome is to reactivate the intact paternal *UBE3A* by suppressing *UBE3A-ATS*. Prior studies show that many neurological phenotypes of maternal *Ube3a* knockout mice can only be rescued by reinstating *Ube3a* expression in early development, indicating a restricted therapeutic window for Angelman syndrome. Here, we report that reducing *Ube3a-ATS* by antisense oligonucleotides in juvenile or adult maternal *Ube3a* knockout mice rescues the abnormal electroencephalogram (EEG) rhythms and sleep disturbance, two prominent clinical features of Angelman syndrome. Importantly, the degree of phenotypic improvement correlates with the increase of *Ube3a* protein levels. These results indicate that the therapeutic window of genetic therapies for Angelman syndrome is broader than previously thought, and EEG power spectrum and sleep architecture should be used to evaluate the clinical efficacy of therapies.

## Editor's evaluation

We believe this study contributes importantly to the literature and in particular, provides support for the potential value of further postnatal rescue experiments in animal models and perhaps future trials in patients.

## Introduction

Angelman syndrome is a rare neurodevelopmental disorder characterized by severe intellectual disability, developmental delay, speech impairment, motor dysfunction, behavioral uniqueness, microcephaly, sleep disturbance, seizures, and abnormal electroencephalogram (EEG) (Williams et al., 2006; Bird, 2014; Buiting et al., 2016). It is caused by loss-of-function of the maternally derived

*UBE3A* gene encoding ubiquitin protein ligase E3A (Kishino et al., 1997; Matsuura et al., 1997). *UBE3A* is expressed from both maternal and paternal alleles in non-neuronal cells, but is paternally imprinted in neurons (Albrecht et al., 1997; Rougeulle et al., 1997; Judson et al., 2014). Imprinted expression of *UBE3A* or silence of the paternal allele in neurons is due to a long non-coding RNA, *UBE3A* antisense transcript (*UBE3A*-ATS). *UBE3A*-ATS is expressed from the paternally inherited chromosome and localized in the nucleus to repress *UBE3A* in *cis* through a transcriptional collision mechanism (Meng et al., 2012; Meng et al., 2013). Thus, loss-of-function of the maternal *UBE3A* leads to the absence of functional *UBE3A* proteins in neurons. Maternal *UBE3A* deficiency can result from deletions in the chromosomal region 15q11–q13 containing *UBE3A*, which account for about 70% of Angelman syndrome patients, mutations in *UBE3A* gene, paternal uniparental disomy of chromosome 15, or an imprinting defect (Williams et al., 2006; Bird, 2014; Buiting et al., 2016).

Studies in rodent models carrying maternal *Ube3a* loss-of-function mutations have provided insights into Angelman syndrome mechanisms and identified therapeutic strategies. Many disease relevant phenotypes were reported in these Angelman syndrome models (Margolis et al., 2015; Rotaru et al., 2020; Yang, 2020), and some of them are robust and reproducible in different models and laboratories, including motor impairments (e.g., poor performance in rotarod and open-field tests), decreased innate marble burying and nest building behaviors, cortical hyperexcitability (e.g., poly-spikes in EEG), altered EEG power spectrum and sleep pattern, increased susceptibility to seizure induction, and reduced synaptic long-term potentiation (Jiang et al., 1998; Miura et al., 2002; Weeber et al., 2003; Colas et al., 2005; Yashiro et al., 2009; Jiang et al., 2010; Huang et al., 2013; Meng et al., 2013; Ehlen et al., 2015; Silva-Santos et al., 2015; Judson et al., 2016; Born et al., 2017; Sidorov et al., 2017; Sonzogni et al., 2018; Gu et al., 2019; Copping and Silverman, 2021). Thus, these phenotypes are suitable for evaluating the effects of potential disease-modifying therapies even though some of them may not be clinically relevant. By genetically reinstating *Ube3a* expression from the maternal allele at different developmental ages, rescue experiments in mice show that most of these neurological functions require *Ube3a* during late embryonic and early postnatal development (Silva-Santos et al., 2015; Rotaru et al., 2018; Gu et al., 2019; Sonzogni et al., 2020), suggesting that the therapeutic window for Angelman syndrome may be limited to very young ages.

Two categories of therapeutic strategies are being actively pursued for Angelman syndrome. One is to target the downstream substrates of *UBE3A* protein, and the other is to restore *UBE3A* gene expression (Margolis et al., 2015; Yang, 2020; Copping et al., 2021; Elgersma and Sonzogni, 2021; Markati et al., 2021). Since the paternal *UBE3A* allele is intact in Angelman syndrome, an attractive approach is to reactivate the silenced paternal *UBE3A* by suppressing *UBE3A*-ATS expression (Figure 1A). Indeed, reducing *Ube3a*-ATS levels in mice through genetic manipulations or topoisomerase inhibition results in unsilencing of the paternal *Ube3a* (Huang et al., 2011; Meng et al., 2012; Meng et al., 2013). Antisense oligonucleotides (ASOs) or CRISPR/Cas9 targeting the mouse *Ube3a*-ATS can also upregulate paternal *Ube3a* expression. Administering ASO or adeno-associated virus (AAV) expressing CRISPR/Cas9 to newborn, but not older, maternal *Ube3a* knockout mice rescues a subset of phenotypes (Meng et al., 2015; Wolter et al., 2020; Milazzo et al., 2021; Schmid et al., 2021). Currently, three Phase 1 or Phase 1/2 clinical trials with ASOs targeting *UBE3A*-ATS are underway. Another approach is to directly express an exogenous copy of *UBE3A* by AAV, which also only rescues a subset of phenotypes of maternal *Ube3a* knockout mice when administered postnatally (Daily et al., 2011; Judson et al., 2021). The reversibility of neurological phenotypes at different ages is summarized in *Supplementary file 1*. These results imply that gene-targeted therapies may have to be administered to late trimester fetuses or newborns to treat Angelman syndrome, as the first postnatal week in mice is generally assumed to be equivalent to the third trimester of human gestation with regard to the central nervous system development (Zeiss, 2021). This timing of intervention would be difficult because currently Angelman syndrome is diagnosed after at least the first 6 months of life and typically between 1 and 4 years of age (Williams et al., 2006).

However, the reversibility of three robust and clinically relevant phenotypes of Angelman mouse models remains untested, namely cortical hyperexcitability (e.g., poly-spikes), altered EEG power spectrum, and sleep disturbance. Alterations in EEG power spectrum, particularly an increase in the power of low frequency oscillations (i.e., 1–30 Hz), are well documented in both Angelman syndrome patients and rodent models (Born et al., 2017; Sidorov et al., 2017; Frohlich et al., 2019; Born et al., 2021; Copping and Silverman, 2021). This brain rhythm is a potential biomarker for assessing

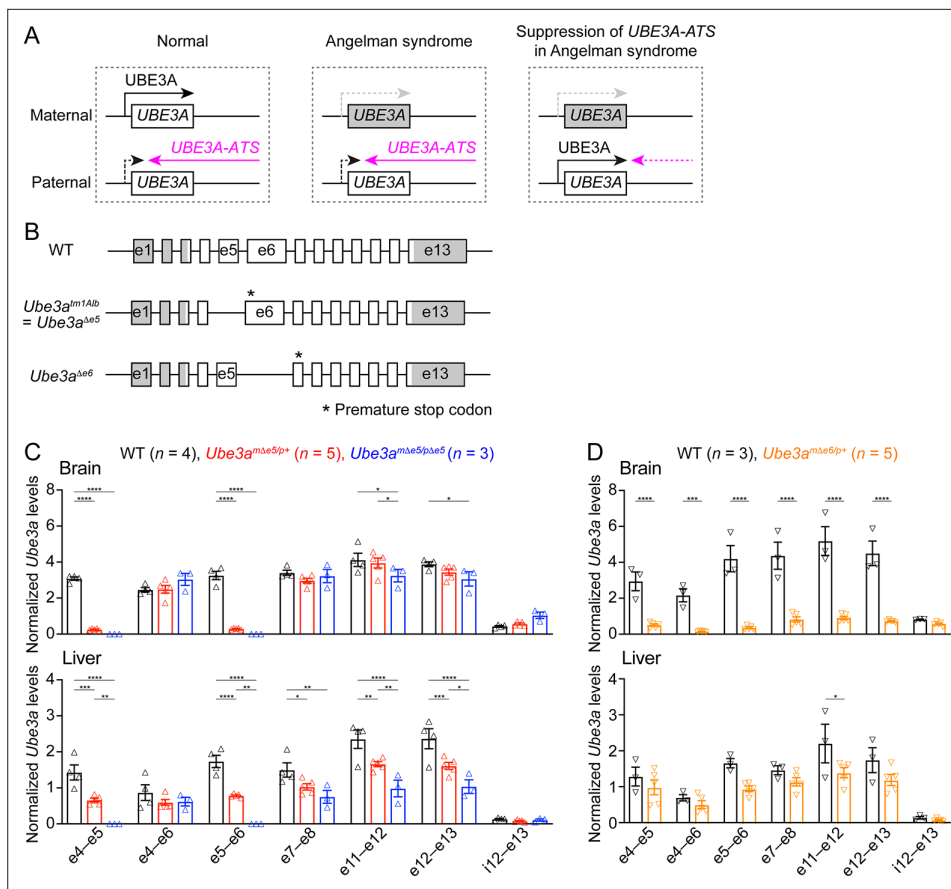


**Figure 1.** *Ube3a* mRNA is diminished in the brain of a new maternal *Ube3a* knockout mouse but remains in a previously generated Angelman syndrome mouse model. **(A)** Schematics of UBE3A imprinting and Angelman syndrome. Left, in normal neurons, UBE3A proteins are only produced from the maternal copy of UBE3A because the paternal copy is silenced by UBE3A-ATS. Middle, deficiency of the maternal UBE3A (gray) leads to the loss of UBE3A proteins in neurons and causes Angelman syndrome. Right, suppressing UBE3A-ATS expression leads to the unsilencing of the paternal UBE3A. **(B)** Genomic structures of *Ube3a* wild-type (WT),  $\Delta e5$  (also known as *tm1Alb*), and  $\Delta e6$  alleles. The boxes indicate exons (e) 1–13. The white and gray regions indicate the coding and non-coding exon sequences of the longest *Ube3a* transcript, respectively. In the  $\Delta e5$  and  $\Delta e6$  alleles, exons 5 and 6 are deleted, resulting in a premature stop codon in exons 6 and 7, respectively. **(C)** *Ube3a* transcript levels were measured from the brains and livers of WT, *Ube3a<sup>Δe5/p+</sup>* and *Ube3a<sup>Δe5/pΔe5</sup>* mice using primer sets targeting different exons or introns as indicated in the figure. *Ube3a* mRNA levels were normalized by the *Gapdh* mRNA levels. Except the deleted exon 5, other exons in the brains of *Ube3a<sup>Δe5/p+</sup>* and *Ube3a<sup>Δe5/pΔe5</sup>* mice remain at the similar levels as WT mice. **(D)** Similar to (C), but for WT and *Ube3a<sup>Δe6/p+</sup>* mice. *Ube3a* transcript is greatly reduced in the *Ube3a<sup>Δe6/p+</sup>* mouse brains. The numbers of tested mice are indicated in the figure. Each symbol represents one mouse. Bar graphs are mean  $\pm$  standard error of the mean (SEM). Two-way analysis of variance (ANOVA) with Tukey (C) or Šídák (D) multiple comparison test for all pairs of groups, \*p < 0.05, \*\*p < 0.01, \*\*\*p < 0.001, \*\*\*\*p < 0.0001.

clinical symptoms because the power in the delta range (2–4 Hz) correlates with symptom severity in Angelman syndrome patients (Hipp et al., 2021; Ostrowski et al., 2021). Similarly, sleep disturbance, another prominent feature of Angelman syndrome (Spruyt et al., 2018), is also recapitulated in the mouse models (Colas et al., 2005; Ehlen et al., 2015; Coping and Silverman, 2021). Hence, to support the ongoing and planned clinical trials, it is crucial to determine to what extent the EEG and sleep deficits are reversible in juvenile and adult Angelman syndrome mouse models because these developmental ages are more clinically relevant than the neonatal period. To address this question, we generated a new mouse *Ube3a* null allele and administered a single dose of ASOs targeting *Ube3a*-ATS to juvenile or adult maternal *Ube3a* knockout mice. We first systematically determined the levels of *Ube3a*-ATS and *Ube3a* transcripts and *Ube3a* proteins across different brain regions at

different timepoints post ASO administration and then evaluated the corresponding EEG and sleep phenotypes.

## Results

### Generation of a new *Ube3a* null allele in mice

Our goal was to assess the effect of *Ube3a*-ATS-targeted ASOs in a mouse model of Angelman syndrome. The widely used mouse model is a *Ube3a* knockout allele (*Ube3a*<sup>tm1Alb</sup>, referred to as *Ube3a*<sup>Δe5</sup> here to be distinguished from the new allele) that deletes exon 5 (previously named as exon 2), resulting in a premature stop codon in exon 6 (Jiang et al., 1998; Figure 1B). We performed reverse transcription droplet digital PCR (RT-ddPCR) analyses on this *Ube3a* knockout allele with primer sets targeting different exons. Exons 4, 6, and other exons downstream of the deleted exon 5 were still transcribed in the brains of adult heterozygous maternal (*Ube3a*<sup>mΔe5/p+</sup>) and homozygous (*Ube3a*<sup>mΔe5/pΔe5</sup>) mutant mice at a level comparable to wild-type (WT) mice (Figure 1C), possibly due to an escape from nonsense-mediated mRNA decay or an alternative start site. Similarly, *Ube3a* mRNA was only modestly reduced in the livers of *Ube3a*<sup>mΔe5/p+</sup> and *Ube3a*<sup>mΔe5/pΔe5</sup> mice (Figure 1C). Although this knockout allele produces very little full-length functional *Ube3a* proteins in the brain (Judson et al., 2014; Grier et al., 2015), we sought to create a new *Ube3a* null allele with diminished *Ube3a* mRNA to facilitate the evaluation of ASO efficacy at the transcript level. CRISPR/Cas9 was used to delete the largest *Ube3a* coding exon, exon 6. The resulting allele (*Ube3a*<sup>Δe6</sup>) carries a premature stop codon in exon 7 (Figure 1B). RT-ddPCR analyses of adult heterozygous maternal mutant mice (*Ube3a*<sup>mΔe6/p+</sup>) showed that *Ube3a* mRNA was diminished in the brain and reduced in the liver as compared to WT mice (Figure 1D). Western blots revealed that *Ube3a* protein levels in different brain regions of *Ube3a*<sup>mΔe6/p+</sup> mice were 2–17% of those in WT mice when they were at 6 weeks of age or older (see below). Thus, both *Ube3a* mRNA and proteins are diminished in the *Ube3a*<sup>mΔe6/p+</sup> mouse brains. Furthermore, *Ube3a*<sup>mΔe6/p+</sup> mice showed similar rotarod and marble burying phenotypes to previously reported deficits in *Ube3a*<sup>mΔe5/p+</sup> mice (Shi et al., 2022).

### ASOs targeting *Ube3a*-ATS non-coding RNA upregulate paternal *Ube3a*-YFP expression

To increase the paternal expression of *Ube3a* in mice, we used two mouse-specific ASOs to downregulate the *Ube3a*-ATS levels. The first one (*Ube3a*-as) is complementary to a region downstream of the *Snord115* small nuclear RNA cluster, and this sequence was also targeted by the 'ASO B' used in a previous study (Meng et al., 2015). The second one (*Snord115*) is complementary to a sequence that repeats 110 times in the *Snord115* RNAs. We first tested these two ASOs in 8-week-old WT mice by administering them via intracerebroventricular (ICV) injection. Both *Ube3a*-as ASO and *Snord115* ASO decreased *Ube3a*-ATS transcripts and increased *Ube3a* mRNA levels (Figure 2—figure supplement 1A, B). To further test the effect on paternal expression of *Ube3a* and visualize the distribution of these two ASOs in the brain, we used paternal *Ube3a*<sup>YFP</sup> mice (*Ube3a*<sup>m+/pYFP</sup>) carrying a yellow fluorescent protein (YFP)-tagged *Ube3a* (Dindot et al., 2008), as downregulating *Ube3a*-ATS is expected to reactivate the paternal *Ube3a*-YFP allele. A non-targeting control ASO, *Ube3a*-as ASO, or *Snord115* ASO was administered to the brains of 3-month-old *Ube3a*<sup>m+/pYFP</sup> mice by a single unilateral ICV injection. We visualized *Ube3a*-YFP expression by immunostaining of YFP 18 days post ASO injection. Maternal *Ube3a*<sup>YFP</sup> mice (*Ube3a*<sup>mYFP/p+</sup>) exhibited strong *Ube3a*-YFP in the brain, whereas *Ube3a*<sup>m+/pYFP</sup> mice receiving the control ASO showed little expression (Figure 2A, B). *Ube3a*-as ASO and *Snord115* ASO increased *Ube3a*-YFP expression in many brain regions of *Ube3a*<sup>m+/pYFP</sup> mice to 40–90% and 20–60% of that of *Ube3a*<sup>mYFP/p+</sup> mice, respectively (Figure 2A, B; Figure 2—figure supplement 1C). Although we did not specifically examine different cell types, YFP was observed in several types of GABAergic neurons including cerebellar Purkinje cells, olfactory bulb granule cells, striatal neurons, and interneurons in cortical layer 1, hippocampal stratum oriens, and cerebellar molecular layer (Figure 2B). Thus, both *Ube3a*-as ASO and *Snord115* ASO can broadly reactivate the paternal *Ube3a*-YFP allele in neurons including GABAergic neurons throughout the mouse brain *in vivo*.

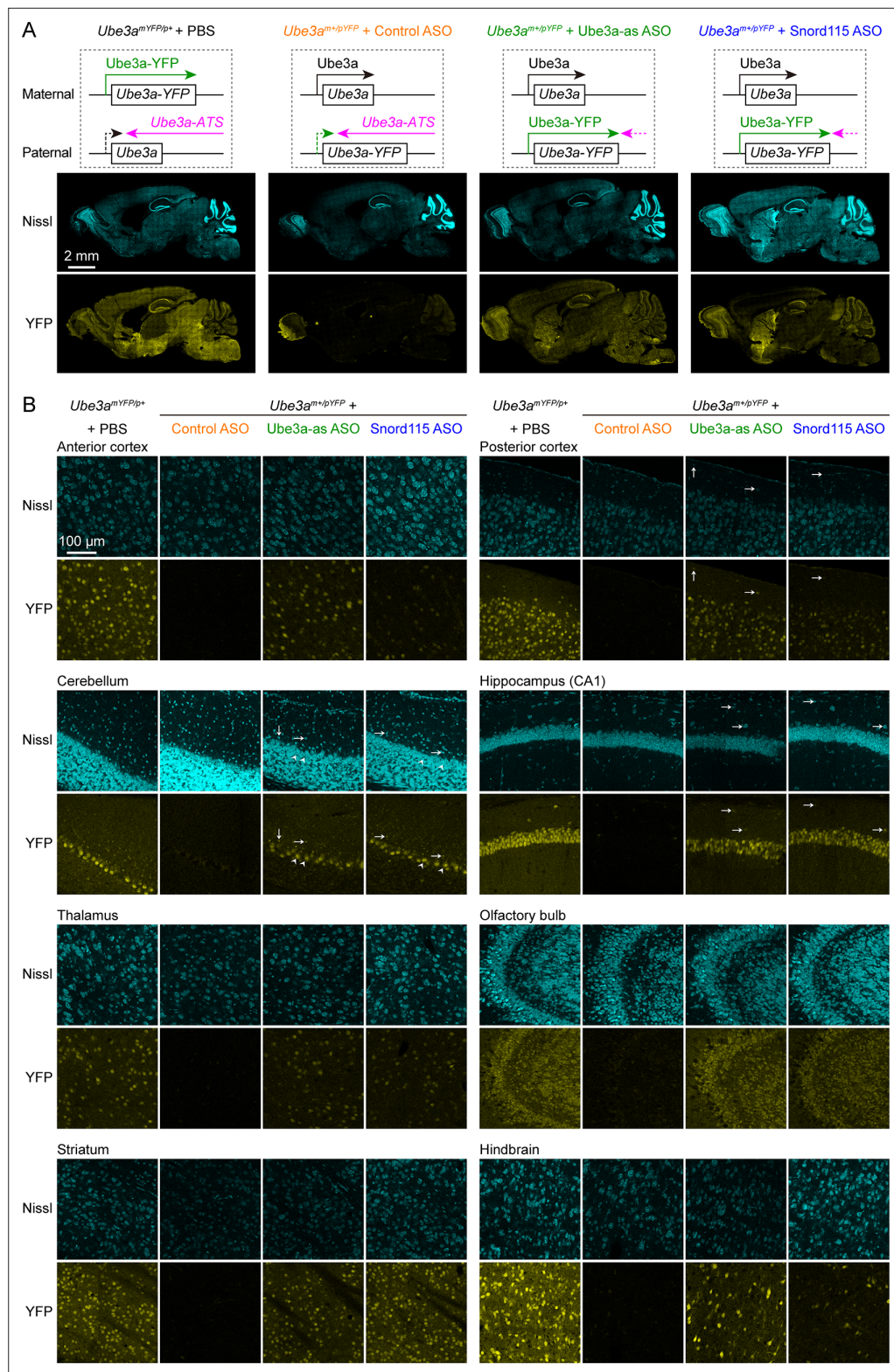


**Figure 2.** Antisense oligonucleotides (ASOs) targeting *Ube3a*-ATS reactivate paternal *Ube3a*-YFP expression. **(A)** Schematics of *Ube3a*-YFP expression (upper panels) and representative fluorescent images of sagittal brain sections (lower panels) from maternal *Ube3a<sup>YFP</sup>* mice (*Ube3a<sup>mYFP/p+</sup>*,  $n = 2$ ) injected with phosphate-buffered saline (PBS) and paternal *Ube3a<sup>YFP</sup>* mice (*Ube3a<sup>m+/pYFP</sup>*) injected with control ( $n = 2$ ), *Ube3a*-as ( $n = 2$ ), or Snord115 ( $n = 2$ ) ASO. Sections were stained with fluorescent Nissl and an antibody recognizing YFP. *Ube3a*-YFP proteins are

Figure 2 continued on next page

*Figure 2 continued*

produced from the maternal copy of *Ube3a*-YFP in *Ube3a<sup>mYFP/p+</sup>* mice, but not from the paternal copy in *Ube3a<sup>m+/pYFP</sup>* mice injected with control ASO because the paternal copy is silenced by *Ube3a*-ATS. Both *Ube3a*-as and Snord115 ASOs can suppress *Ube3a*-ATS expression in *Ube3a<sup>m+/pYFP</sup>* mice and broadly reactivate the paternal *Ube3a*-YFP expression in the brains. (B) Similar to (A), but for images of eight different brain regions at high magnification. Arrows indicate YFP-positive GABAergic interneurons in cortical layer 1, cerebellar molecular layer, and hippocampal stratum oriens. Arrow heads indicate YFP-positive cerebellar Purkinje cells.

The online version of this article includes the following figure supplement(s) for figure 2:

**Figure supplement 1.** Antisense oligonucleotides (ASOs) targeting *Ube3a*-ATS increase *Ube3a* transcripts in wild-type (WT) mice and *Ube3a*-YFP expression in *Ube3a<sup>m+/pYFP</sup>* mice.

### ***Ube3a*-as ASO and Snord115 ASO reactivate paternal *Ube3a* expression in *Ube3a<sup>mΔe6/p+</sup>* mice**

We sought to assess the efficacy of *Ube3a*-as ASO and Snord115 ASO in our new mouse model of Angelman syndrome across brain regions and over time by systematically determining the total *Ube3a* protein, *Ube3a* mRNA, and *Ube3a*-ATS levels. We first injected male and female *Ube3a<sup>mΔe6/p+</sup>* mice with control, *Ube3a*-as, or Snord115 ASO and their sex- and age-matched WT littermates with control ASO in parallel at the juvenile age (postnatal days  $21.9 \pm 0.1$  [mean  $\pm$  standard error of the mean, SEM], range 21–24,  $n = 91$ ). Brain tissues were harvested from eight different regions of both hemispheres at 3, 6, and 10 weeks post ASO injection (**Figure 3A**). We used the hemispheres ipsilateral to the ASO injection site for Western blot analyses and the corresponding contralateral hemispheres for reverse transcription quantitative real-time PCR (RT-qPCR) analyses. At 3 weeks post ASO injection, *Ube3a*-as ASO and Snord115 ASO increased *Ube3a* protein levels in *Ube3a<sup>mΔe6/p+</sup>* mice to about 28–71% of the WT levels in different brain regions (**Figure 3B, D, E; Figure 3—figure supplement 1A; Figure 3—figure supplement 2**). Correlated with this result, *Ube3a*-ATS levels were downregulated by 29–73% (**Figure 4A, B; Figure 4—figure supplement 1**) and *Ube3a* mRNA levels were increased to about 22–57% of the WT levels (**Figure 4A, B; Figure 4—figure supplement 1**). The effects of *Ube3a*-as ASO remained stable for at least 10 weeks. However, the *Ube3a* protein and *Ube3a* mRNA levels in Snord115 ASO-treated *Ube3a<sup>mΔe6/p+</sup>* mice markedly decreased at 6 weeks post injection and reached to the levels of control ASO-treated *Ube3a<sup>mΔe6/p+</sup>* mice in most brain regions by 10 weeks post injection (**Figure 3B, D, E; Figure 3—figure supplement 1A; Figure 3—figure supplement 2; Figure 4A, B; Figure 4—figure supplement 1**). Correspondingly, by 10 weeks post injection the *Ube3a*-ATS levels in the Snord115 ASO-treated *Ube3a<sup>mΔe6/p+</sup>* mice returned to those in control ASO-treated WT or *Ube3a<sup>mΔe6/p+</sup>* mice (**Figure 4A, B; Figure 4—figure supplement 1**).

We further tested the ASOs in adult mice (postnatal days  $64.6 \pm 0.5$  [mean  $\pm$  SEM], range 56–72,  $n = 83$ ). At 3 weeks post ASO injection, *Ube3a*-as ASO and Snord115 ASO also significantly reduced *Ube3a*-ATS levels and increased *Ube3a* mRNA and *Ube3a* protein levels in *Ube3a<sup>mΔe6/p+</sup>* mice (**Figure 3C, D, F; Figure 3—figure supplement 1B; Figure 3—figure supplement 2; Figure 4A, B; Figure 4—figure supplement 1**). However, the upregulation of *Ube3a* proteins appeared to be slightly less effective in some brain regions (e.g., posterior cortex, thalamus and hypothalamus, and midbrain and hindbrain) than injecting ASOs to juvenile mice (**Figure 3E, F**). Furthermore, the effects of *Ube3a*-as ASO modestly decreased over the course of 10 weeks post injection, and the reduction in efficacies over time was much more evident for Snord115 ASO (**Figure 3F; Figure 4A, B; Figure 4—figure supplement 1**).

*Ube3a* gene in mice produces two *Ube3a* protein isoforms that differ by 21 amino acids at the N terminus. The short *Ube3a* isoform 3 is the dominant isoform and mainly localized in the nucleus, whereas the long isoform 2 is expressed at 20–30% of the isoform 3 level and primarily distributed in the cytosol (**Miao et al., 2013; Avagliano Trezza et al., 2019**). Mice selectively lacking the *Ube3a* isoform 3 recapitulate several key phenotypes of maternal *Ube3a* knockout mice, showing the critical role of the nuclear *Ube3a* isoform 3 in Angelman syndrome (**Avagliano Trezza et al., 2019**). Thus, we performed additional Western blot analyses and found that both *Ube3a* isoforms were similarly upregulated by *Ube3a*-as ASO or Snord115 ASO in different brain regions of *Ube3a<sup>mΔe6/p+</sup>* mice (**Figure 3—figure supplement 3; Figure 3—figure supplement 4**), confirming the successful reactivation of the critical isoform 3.

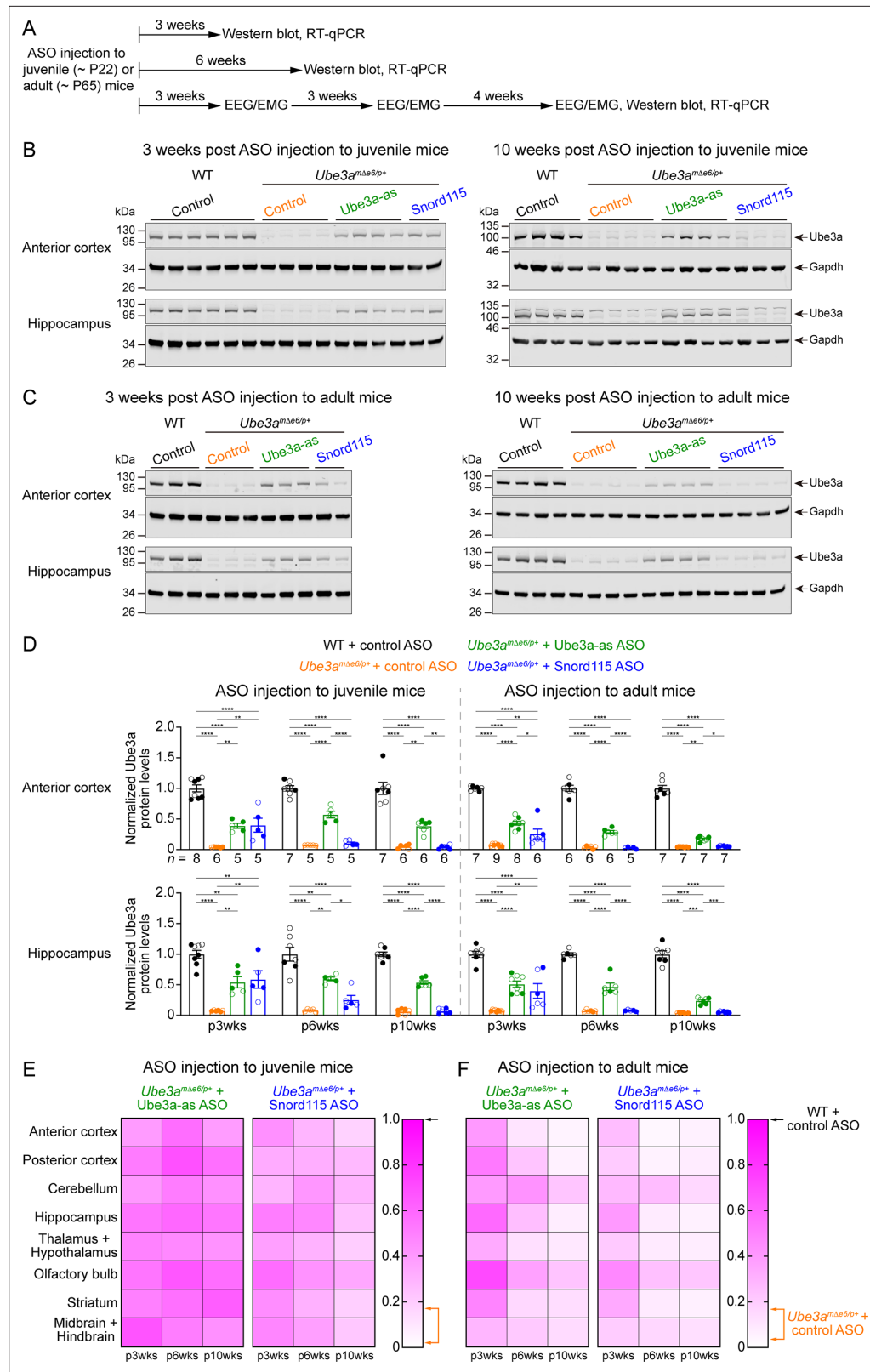


**Figure 3.** Antisense oligonucleotides (ASOs) targeting *Ube3a*-ATS upregulate *Ube3a* protein in *Ube3a<sup>mΔe6/p+</sup>* mice.  
**(A)** Experimental designs and timelines. ASOs were injected into three cohorts of juvenile mice around postnatal day 22 (P22). Protein and RNA were measured from two cohorts of mice at 3 and 6 weeks post ASO injection. Electroencephalogram (EEG) and electromyogram (EMG) were measured from the third cohort of mice at 3, 6, and 10 weeks post ASO injection.

Figure 3 continued on next page

*Figure 3 continued*

10 weeks post ASO injection, and protein and RNA were measured after the last EEG/EMG recording. The same experiments were performed for three cohorts of adult mice injected with ASOs around P65. **(B, C)** ASOs were injected into juvenile (**B**) or adult (**C**) mice. Representative Western blots at 3 and 10 weeks post ASO injection from the anterior cortex and hippocampus of wild-type (WT) mice injected with control ASO and *Ube3a*<sup>mΔe6/p+</sup> mice with control, *Ube3a*-as, or Snord115 ASO. Gapdh, a housekeeping protein as loading control. **(D)** Summary data of normalized *Ube3a* protein levels from the anterior cortex (upper panel) and hippocampus (lower panel) at 3, 6, and 10 weeks post ASO injection indicated by p3wks, p6wks, and p10wks, respectively. *Ube3a* levels were first normalized by the Gapdh levels and then by the average *Ube3a* levels of all WT mice from the same blot. *Ube3a* levels are diminished in control ASO-treated *Ube3a*<sup>mΔe6/p+</sup> mice as compared to control ASO-treated WT mice. The upregulation of *Ube3a* protein by *Ube3a*-as ASO is evident up to 10 weeks post ASO injection, whereas the effect of Snord115 ASO diminishes over time. The numbers of tested mice are indicated in the figure. Each filled (male) or open (female) circle represents one mouse. Bar graphs are mean ± standard error of the mean (SEM). One-way analysis of variance (ANOVA) with Tukey multiple comparison test for all pairs of groups, \*p < 0.05, \*\*p < 0.01, \*\*\*p < 0.001, \*\*\*\*p < 0.0001. **(E, F)** Heat maps showing the normalized *Ube3a* protein levels from different brain regions of *Ube3a*-as or Snord115 ASO-treated juvenile (**E**) and adult (**F**) *Ube3a*<sup>mΔe6/p+</sup> mice at 3, 6, and 10 weeks post ASO injection. In the color scales, 1 represents the *Ube3a* levels in control ASO-treated WT mice for each brain region (black arrows), and the orange arrows indicate the range of *Ube3a* levels in control ASO-treated *Ube3a*<sup>mΔe6/p+</sup> mice.

The online version of this article includes the following source data and figure supplement(s) for figure 3:

**Source data 1.** Raw images of the Western blots in **Figure 3B**.

**Source data 2.** Raw images of the Western blots in **Figure 3C**.

**Figure supplement 1.** Antisense oligonucleotides (ASOs) targeting *Ube3a*-ATS upregulate *Ube3a* protein in different brain regions of *Ube3a*<sup>mΔe6/p+</sup> mice (Part I).

**Figure supplement 1—source data 1.** Raw images of the Western blots in **Figure 3—figure supplement 1A**, left panels.

**Figure supplement 1—source data 2.** Raw images of the Western blots in **Figure 3—figure supplement 1A**, right panels.

**Figure supplement 1—source data 3.** Raw images of the Western blots in **Figure 3—figure supplement 1B**, left panels.

**Figure supplement 1—source data 4.** Raw images of the Western blots in **Figure 3—figure supplement 1B**, right panels.

**Figure supplement 2.** Antisense oligonucleotides (ASOs) targeting *Ube3a*-ATS upregulate *Ube3a* protein in different brain regions of *Ube3a*<sup>mΔe6/p+</sup> mice (Part II).

**Figure supplement 3.** *Ube3a* isoforms 2 and 3 are similarly upregulated by *Ube3a*-ATS-targeted antisense oligonucleotides (ASOs) in juvenile *Ube3a*<sup>mΔe6/p+</sup> mice.

**Figure supplement 3—source data 1.** Raw images of the Western blots in **Figure 3—figure supplement 3A**, upper panels.

**Figure supplement 3—source data 2.** Raw images of the Western blots in **Figure 3—figure supplement 3A**, lower panels.

**Figure supplement 4.** *Ube3a* isoforms 2 and 3 are similarly upregulated by *Ube3a*-ATS-targeted antisense oligonucleotides (ASOs) in adult *Ube3a*<sup>mΔe6/p+</sup> mice.

**Figure supplement 4—source data 1.** Raw images of the Western blots in **Figure 3—figure supplement 4A**, upper panels.

**Figure supplement 4—source data 2.** Raw images of the Western blots in **Figure 3—figure supplement 4A**, lower panels.

**Figure supplement 5.** Similar increase of *Ube3a* protein by two different doses of antisense oligonucleotides (ASOs) in *Ube3a*<sup>mΔe6/p+</sup> mice.

Finally, we examined the relationships among total *Ube3a*-ATS, *Ube3a* mRNA, and *Ube3a* protein levels across individual mice and timepoints. *Ube3a*-ATS levels negatively correlated with *Ube3a* protein and *Ube3a* mRNA levels in *Ube3a*<sup>mΔe6/p+</sup> mice (**Figure 4C**; **Figure 4—figure supplement 2A**), and *Ube3a* protein levels positively correlated with *Ube3a* mRNA levels (**Figure 4—figure supplement 2B**). Since the protein and transcript levels were measured at the same post ASO injection timepoints from the ipsilateral and contralateral hemispheres, respectively, these correlations indicate a broad distribution of ASOs in the mouse brains and a spatiotemporally comparable pattern between

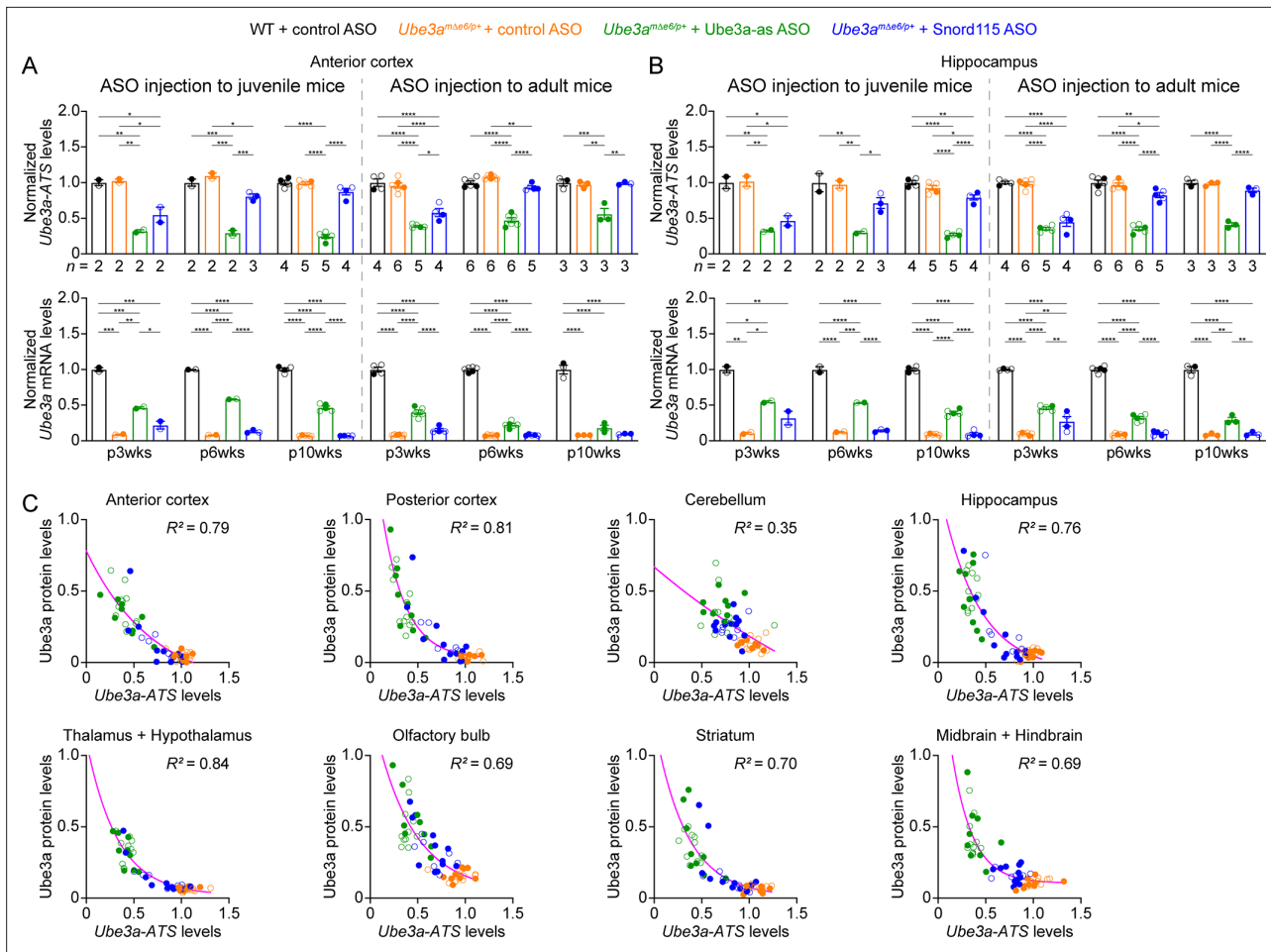


**Figure 4.** Antisense oligonucleotides (ASOs) targeting *Ube3a*-ATS reduce *Ube3a*-ATS and increase *Ube3a* transcripts in *Ube3a*<sup>mΔe6/p+</sup> mice. **(A, B)** Juvenile or adult wild-type (WT) mice were injected with control ASO and *Ube3a*<sup>mΔe6/p+</sup> mice with control, *Ube3a-as*, or *Snord115* ASO. Summary data show the normalized *Ube3a*-ATS (upper panels) and *Ube3a* (lower panels) transcript levels from the anterior cortex (**A**) and hippocampus (**B**) at 3, 6, and 10 weeks post ASO injection indicated by p3wks, p6wks, and p10wks, respectively. *Ube3a*-ATS and *Ube3a* mRNA levels were first normalized by the *Gapdh* levels and then by the average *Ube3a*-ATS and *Ube3a* mRNA levels of all WT mice, respectively. The downregulation of *Ube3a*-ATS and upregulation of *Ube3a* mRNA by *Ube3a-as* ASO are evident up to 10 weeks post ASO injection, whereas the effect of *Snord115* ASO diminishes over time. The numbers of tested mice are indicated in the figure. Bar graphs are mean ± standard error of the mean (SEM). One-way analysis of variance (ANOVA) with Tukey multiple comparison test for all pairs of groups, \*p < 0.05, \*\*p < 0.01, \*\*\*p < 0.001, \*\*\*\*p < 0.0001. **(C)** The negative correlations between *Ube3a*-ATS transcript levels and *Ube3a* protein levels from different brain regions of *Ube3a*<sup>mΔe6/p+</sup> mice injected with control, *Ube3a-as*, or *Snord115* ASO were fitted with a one phase exponential decay ( $Y = ae^{-kX} + b$ ; X, *Ube3a*-ATS transcript levels; Y, *Ube3a* protein levels; a, b, k, constants). Data from 3, 6, and 10 weeks post ASO injection into juvenile and adult mice were all included. Each filled (male) or open (female) circle represents one mouse. R<sup>2</sup> indicates the goodness of fit.

The online version of this article includes the following figure supplement(s) for figure 4:

**Figure supplement 1.** Antisense oligonucleotides (ASOs) targeting *Ube3a*-ATS reduce *Ube3a*-ATS and increase *Ube3a* transcripts in different brain regions of *Ube3a*<sup>mΔe6/p+</sup> mice (Part I).

**Figure supplement 2.** Antisense oligonucleotides (ASOs) targeting *Ube3a*-ATS reduce *Ube3a*-ATS and increase *Ube3a* transcripts in different brain regions of *Ube3a*<sup>mΔe6/p+</sup> mice (Part II).

the changes in transcripts and proteins. Taken together, our results demonstrate that a single unilateral ICV injection of ASO targeting *Ube3a*-ATS in *Ube3a*<sup>mΔe6/p+</sup> mice leads to a long-lasting downregulation of this transcript and reactivation of the paternal *Ube3a* allele throughout the brains, and the upregulation of *Ube3a* proteins by *Ube3a-as* ASO can last at least 10 weeks.

## Reactivation of paternal *Ube3a* expression alleviates abnormal EEG rhythmic activity in *Ube3a*<sup>mΔe6/p+</sup> mice

Maternal *Ube3a* deficiency in mice causes altered brain rhythms, sleep disturbance, and epileptiform activity (e.g., cortical poly-spikes), all of which can be examined by chronic video-EEG and electromyogram (EMG) recordings. Thus, to determine if upregulation of paternal *Ube3a* expression can reverse these phenotypes in *Ube3a*<sup>mΔe6/p+</sup> mice, we injected male and female *Ube3a*<sup>mΔe6/p+</sup> mice with control, *Ube3a*-as, or Snord115 ASO and their sex- and age-matched WT littermates with control ASO in parallel at the juvenile (postnatal days 21.5 ± 0.1 [mean ± SEM], range 21–24,  $n = 35$ ) or adult (postnatal days 62.5 ± 0.6 [mean ± SEM], range 56–66,  $n = 28$ ) age. Intracranial EEG from the frontal, somatosensory, and visual cortices and EMG from the neck muscles of each mouse were recorded at 3, 6, and 10 weeks post ASO injection (**Figure 3A**, **Figure 5A**). To avoid bias, we evenly sampled 6 out of 24 hr of the EEG/EMG data for power spectrum and poly-spikes analyses and used 24 hr of data for sleep scoring (see Materials and methods).

We first removed artifacts and then computed the absolute power spectral densities (PSDs) of EEG signals including all brain states (**Figure 5—figure supplement 1**). To control for the variations caused by different impedances across electrodes and mice, we normalized PSDs by the total power within 1–100 Hz to obtain the relative PSDs. The relative PSDs from the frontal cortex of control ASO-treated *Ube3a*<sup>mΔe6/p+</sup> mice were higher at 4–25 Hz and lower at 40–100 Hz than those of control ASO-treated WT mice (**Figure 5B–D, F–H; Figure 5—figure supplement 2**). Thus, we further computed the relative power in the frequency bands of delta ( $\delta$ , 1–4 Hz), theta ( $\theta$ , 4–8 Hz), alpha ( $\alpha$ , 8–13 Hz), low beta ( $\beta_1$ , 13–18 Hz), high beta ( $\beta_2$ , 18–25 Hz), low gamma ( $\gamma_1$ , 25–50 Hz), and high gamma ( $\gamma_2$ , 50–100 Hz). To capture the concurrent changes in both low- and high-frequency ranges, we calculated the ratio of the total power in the alpha, low beta, and high beta bands over the power in high gamma band (i.e.,  $(\alpha + \beta_1 + \beta_2)/\gamma_2$ ). This ratio represents the relative distribution of power between the low- and high-frequency bands and importantly, is independent from the use of PSD or relative PSD. We discovered that the power ratio  $(\alpha + \beta_1 + \beta_2)/\gamma_2$  was higher in control ASO-treated *Ube3a*<sup>mΔe6/p+</sup> mice than control ASO-treated WT mice across all timepoints (**Figure 5E, I**). Similar phenotypes were also observed in the somatosensory cortex (**Figure 5—figure supplement 3**), but the EEG rhythmic activity in the visual cortex was not significantly altered in control ASO-treated *Ube3a*<sup>mΔe6/p+</sup> mice (**Figure 5—figure supplement 4**). These results indicate that maternal *Ube3a* deficiency alters EEG rhythms in the frontal and somatosensory cortices, and the power ratio  $(\alpha + \beta_1 + \beta_2)/\gamma_2$  can be a robust measure of the effects of *Ube3a*-as and Snord115 ASOs.

Treating *Ube3a*<sup>mΔe6/p+</sup> mice with *Ube3a*-as ASO at the juvenile age caused a decrease of the power in the alpha, low beta, and high beta bands and an increase of the power in the high gamma band, particularly at 3 and 6 weeks post ASO injection (**Figure 5B–D; Figure 5—figure supplement 2A; Figure 5—figure supplement 3A, B**), which led to the normalization of the ratio  $(\alpha + \beta_1 + \beta_2)/\gamma_2$  in the frontal and somatosensory cortices, as the ratios in *Ube3a*-as ASO-treated *Ube3a*<sup>mΔe6/p+</sup> mice were indistinguishable from those in control ASO-treated WT mice (**Figure 5E; Figure 5—figure supplement 3C**). In contrast, Snord115 ASO only showed such effects in the frontal cortex at 3 weeks post ASO injection, and the effects waned at later timepoints (**Figure 5E; Figure 5—figure supplement 3C**). This difference between *Ube3a*-as ASO and Snord115 ASO generally correlates with their difference in upregulating *Ube3a* proteins (see below). When *Ube3a*<sup>mΔe6/p+</sup> mice were treated with ASOs at the adult age, *Ube3a*-as ASO and Snord115 ASO were also able to reduce the power in the low frequency bands and increased the power in the high gamma band in the frontal cortex (**Figure 5F–H; Figure 5—figure supplement 2B**), thereby reducing the ratio  $(\alpha + \beta_1 + \beta_2)/\gamma_2$  (**Figure 5I**). These effects also waned over time, consistent with the change of *Ube3a* protein levels (**Figure 3F**). Altogether, these results show that upon reactivation of the paternal *Ube3a* by *Ube3a*-ATS-targeted ASOs in juvenile or adult *Ube3a*<sup>mΔe6/p+</sup> mice, the abnormal EEG rhythmic activity in *Ube3a*<sup>mΔe6/p+</sup> mice can be reversed in a *Ube3a* protein level-dependent manner.

## Reactivation of paternal *Ube3a* expression restores normal sleep pattern in *Ube3a*<sup>mΔe6/p+</sup> mice

To study the sleep architecture, we used the EEG and EMG signals and a convolutional neural network-based algorithm SPINDLE (**Miladinović et al., 2019**) to classify the brain states into rapid eye movement (REM) sleep, non-rapid eye movement (NREM) sleep, and wake throughout 24 hr

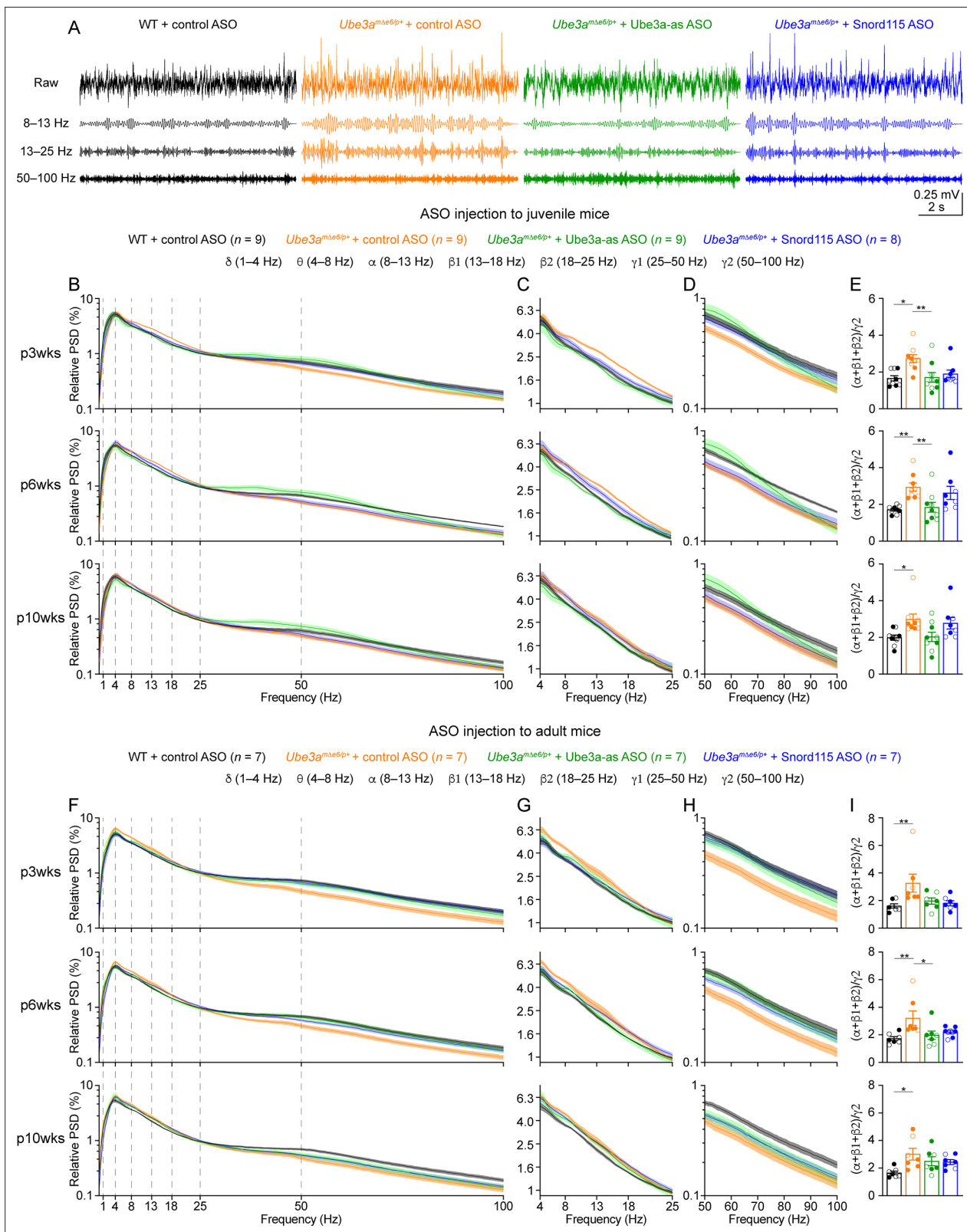


**Figure 5.** Reactivation of paternal *Ube3a* rescues abnormal electroencephalogram (EEG) rhythms in *Ube3a<sup>mΔe6/p+</sup>* mice. **(A)** Juvenile wild-type (WT) mice were injected with control antisense oligonucleotide (ASO) and *Ube3a<sup>mΔe6/p+</sup>* mice with control, Ube3a-as, or Snord115 ASO. Representative raw EEG traces and their band-pass filtered traces from the left frontal cortices at 6 weeks post ASO injection. **(B–D)** Relative EEG power spectral density (PSD) curves from the left front cortices at 3, 6, and 10 weeks post ASO injection indicated by p3wks, p6wks, and p10wks, respectively. The dashed

Figure 5 continued on next page

**Figure 5 continued**

lines indicate different frequency bands (**B**). The expanded theta ( $\theta$ )–high beta ( $\beta_2$ ) and high gamma ( $\gamma_2$ ) bands are shown in (**C**) and (**D**). Lines and shades are mean and standard error of the mean (SEM), respectively. Control ASO-treated  $Ube3a^{m\Delta e6/p+}$  mice show an increase of power in the 8–25 Hz range and a decrease of power in the 50–100 Hz range as compared to control ASO-treated WT mice.  $Ube3a$ -as ASO reduces the power in 8–25 Hz and increases the power in 50–100 Hz in  $Ube3a^{m\Delta e6/p+}$  mice. Snord115 ASO has a similar effect in  $Ube3a^{m\Delta e6/p+}$  mice at 3 weeks post ASO injection. See **Figure 5—figure supplement 2** for statistical comparisons. (**E**) Summary data show the ratio of power in 8–25 over 50–100 Hz. Control ASO-treated  $Ube3a^{m\Delta e6/p+}$  mice show a higher ratio than control ASO-treated WT mice.  $Ube3a$ -as ASO reduces the ratio in  $Ube3a^{m\Delta e6/p+}$  mice. Snord115 ASO has a similar effect at 3 weeks post ASO injection. (**F–I**) Similar to (**B–E**), but for ASO injection into adult mice. Note,  $Ube3a$ -as ASO reduces the ratio of power in 8–25 Hz over 50–100 Hz in  $Ube3a^{m\Delta e6/p+}$  mice. The numbers of tested mice are indicated in the figure. Each filled (male) or open (female) circle represents one mouse. Bar graphs are mean  $\pm$  SEM. Kruskal–Wallis test with Dunn's multiple comparison test (**E, I**) for all pairs of groups, \* $p < 0.05$ , \*\* $p < 0.01$ .

The online version of this article includes the following figure supplement(s) for figure 5:

**Figure supplement 1.** Absolute power spectral densities (PSDs) of electroencephalogram (EEG) signals from different brain regions.

**Figure supplement 2.** Reactivation of paternal  $Ube3a$  in  $Ube3a^{m\Delta e6/p+}$  mice restores the relative power in different electroencephalogram (EEG) frequency bands.

**Figure supplement 3.** Reactivation of paternal  $Ube3a$  rescues abnormal electroencephalogram (EEG) rhythms in the somatosensory cortex of  $Ube3a^{m\Delta e6/p+}$  mice.

**Figure supplement 4.** Normal electroencephalogram (EEG) rhythms in the visual cortex of  $Ube3a^{m\Delta e6/p+}$  mice.

(**Figure 6—figure supplement 1A**). The difference in the EEG PSDs did not affect the accuracy of SPINDLE (**Figure 6—figure supplement 1B, C**). Overall, mice spent more time in REM and NREM sleep and less time in wake during the light phase than the dark phase (**Figure 6**). The time in wake was similar between control ASO-treated WT and  $Ube3a^{m\Delta e6/p+}$  mice across ages (**Figure 6C, F**). Control ASO-treated  $Ube3a^{m\Delta e6/p+}$  mice spent significantly less time in REM sleep than control ASO-treated WT mice in the light phase, but this phenotype was more variable in adult mice (**Figure 6A, D**). Correspondingly, control ASO-treated  $Ube3a^{m\Delta e6/p+}$  mice spent slightly more time in NREM sleep than control ASO-treated WT mice because REM sleep is a small fraction of the total sleep (**Figure 6B, E**). Thus, the sleep disturbance in  $Ube3a^{m\Delta e6/p+}$  mice manifests as a selective reduction in REM sleep, which recapitulates the observation in Angelman patients (**Miano et al., 2004; Miano et al., 2005**).

Administering  $Ube3a$ -as ASO or Snord115 ASO to juvenile  $Ube3a^{m\Delta e6/p+}$  mice increased their time in REM sleep at 3 and 6 weeks post ASO injection, thereby normalizing their sleep pattern, as their time in REM sleep was indistinguishable from that in control ASO-treated WT mice (**Figure 6A**). This effect was reduced at 10 weeks post ASO injection (**Figure 6A**). When  $Ube3a^{m\Delta e6/p+}$  mice were treated with ASOs at the adult age,  $Ube3a$ -as ASO and Snord115 ASO were less effective in restoring REM sleep (**Figure 6D**). Overall, these results indicate that the sleep disturbance in  $Ube3a^{m\Delta e6/p+}$  mice can be rescued by reactivation of the paternal  $Ube3a$  in juvenile mice.

### Partial restoration of $Ube3a$ protein levels does not suppress cortical hyperexcitability in $Ube3a^{m\Delta e6/p+}$ mice

Most Angelman syndrome patients develop epileptic seizures within the first 3 years of age (**Williams et al., 2006; Bird, 2014**). Although maternal  $Ube3a$  knockout mice or rats do not develop spontaneous seizures, they exhibit cortical hyperexcitability and epileptiform activity, manifesting as numerous poly-spikes (**Mandel-Brehm et al., 2015; Born et al., 2017; Born et al., 2021**). Indeed, control ASO-treated  $Ube3a^{m\Delta e6/p+}$  mice showed significantly more poly-spikes in the frontal and somatosensory cortices than control ASO-treated WT mice (**Figure 7A–C; Figure 7—figure supplement 1A, C**). Interestingly, the visual cortices of control ASO-treated  $Ube3a^{m\Delta e6/p+}$  mice did not exhibit this epileptiform activity (**Figure 7—figure supplement 1B, D**).  $Ube3a$ -as ASO or Snord115 ASO treatment of juvenile  $Ube3a^{m\Delta e6/p+}$  mice did not significantly reduce poly-spikes as compared to control ASO, although Snord115 ASO-treated  $Ube3a^{m\Delta e6/p+}$  mice showed a 50% reduction in the number of poly-spikes (**Figure 7B; Figure 7—figure supplement 1A**). Similarly, treating adult  $Ube3a^{m\Delta e6/p+}$  mice with  $Ube3a$ -as ASO or Snord115 ASO did not cause a significant decrease of poly-spikes at any timepoint (**Figure 7C; Figure 7—figure supplement 1C**). Thus, these results indicate that under our experimental conditions where  $Ube3a$  protein levels are partially restored in juvenile or adult  $Ube3a^{m\Delta e6/p+}$  mice, their cortical hyperexcitability phenotype cannot be reversed.

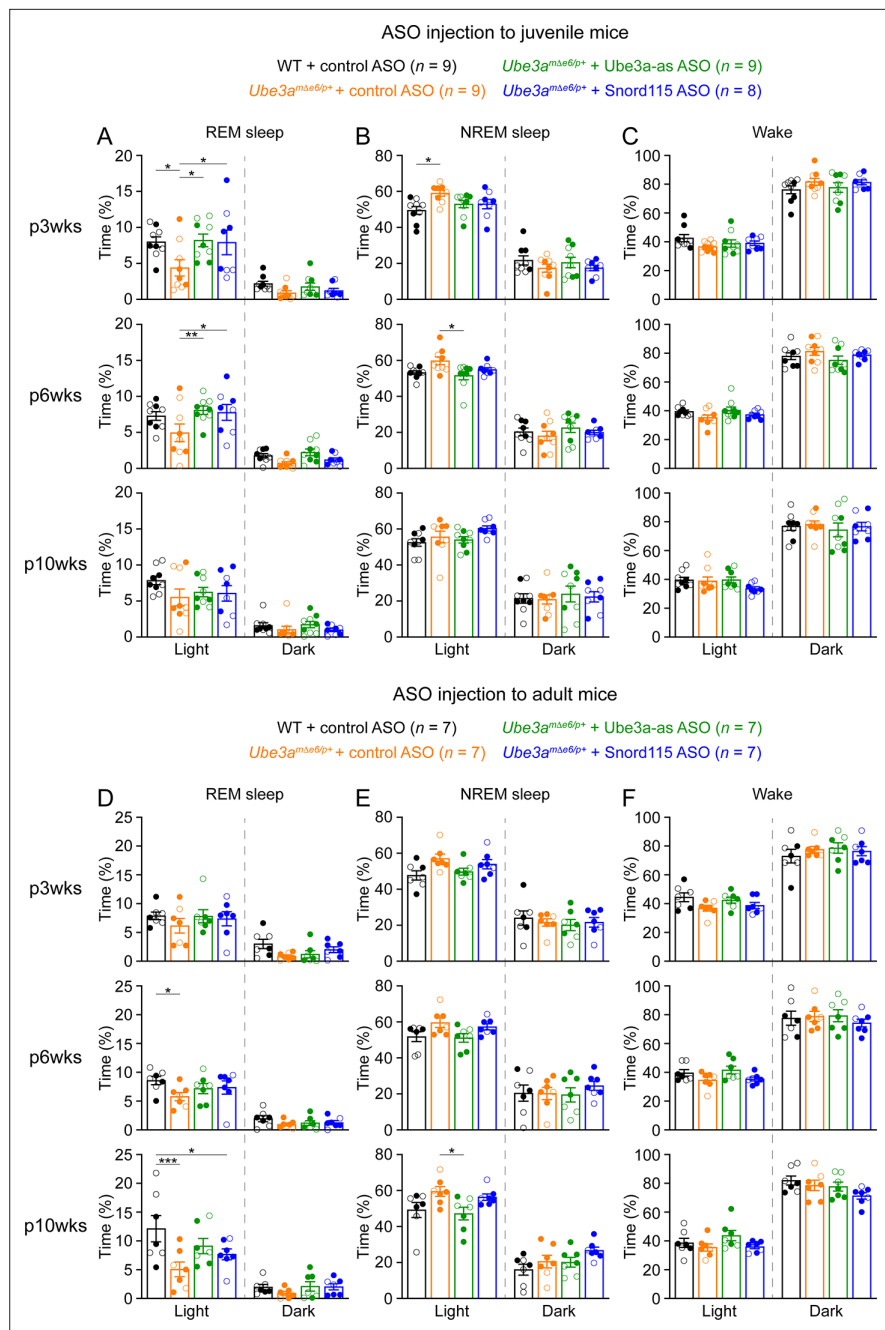


**Figure 6.** Reactivation of paternal *Ube3a* rescues abnormal rapid eye movement (REM) sleep in *Ube3a*<sup>mΔe6/p+</sup> mice. (A) Summary data of the cumulative REM sleep time at 3, 6, and 10 weeks post antisense oligonucleotide (ASO) injection into juvenile mice. Control ASO-treated *Ube3a*<sup>mΔe6/p+</sup> mice spend less time in REM sleep than control ASO-treated wild-type (WT) mice. Both *Ube3a*-as and Snord115 ASOs improve REM sleep in *Ube3a*<sup>mΔe6/p+</sup> mice. (B, C) Similar to (A), but for non-rapid eye movement (NREM) sleep (B) and wake (C). (D–F) Similar to (A–C), but for ASO injection into adult mice. The rescue effect of *Ube3a*-as and Snord115 ASOs is reduced as compared to ASO injection into juvenile mice. The numbers of tested mice are indicated in the figure. Each filled (male) or open (female) circle represents one mouse. Bar graphs are mean  $\pm$  standard error of the mean (SEM). Two-way analysis of variance (ANOVA) with Tukey multiple comparison test for all pairs of groups, \**p* < 0.05, \*\**p* < 0.01, \*\*\**p* < 0.001.

The online version of this article includes the following figure supplement(s) for figure 6:

**Figure supplement 1.** Validation of sleep staging by SPINDLE program.

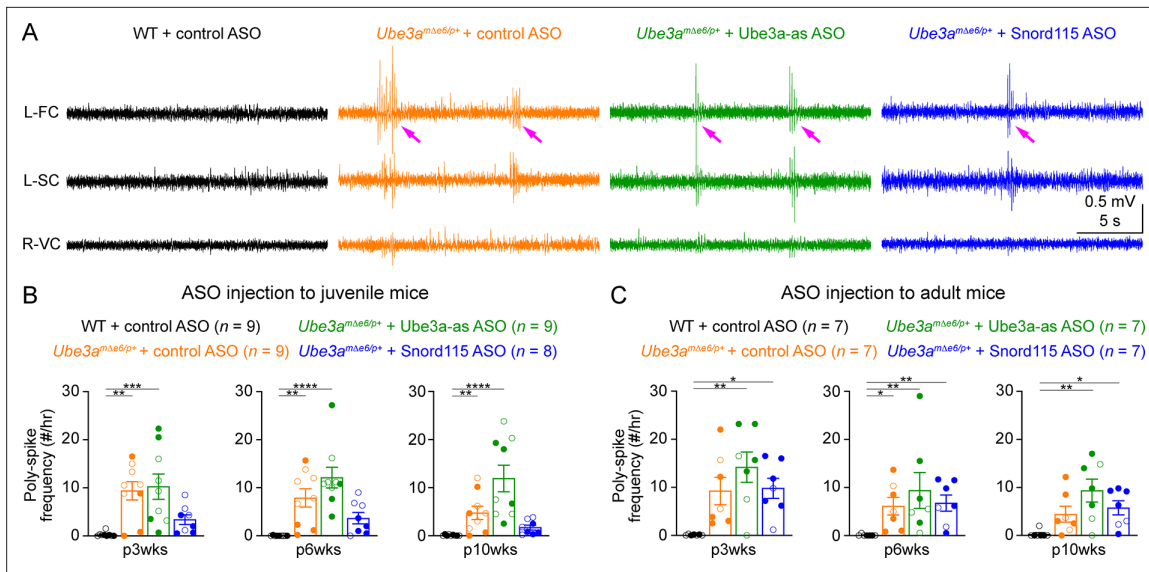


**Figure 7.** Reactivation of paternal *Ube3a* does not suppress poly-spikes in *Ube3a*<sup>Δe6/p+</sup> mice. **(A)** Representative electroencephalogram (EEG) traces from the left frontal cortices (L-FC), left somatosensory cortices (L-SC), and right visual cortices (R-VC) at 3 weeks post antisense oligonucleotide (ASO) injection into juvenile mice. **(B)** Summary data showing the frequencies of poly-spikes from the left frontal cortices at 3, 6, and 10 weeks post ASO injection into juvenile mice. Control ASO-treated *Ube3a*<sup>Δe6/p+</sup> mice show many more poly-spikes than control ASO-treated wild-type (WT) mice. Snord115 ASO modestly reduces poly-spikes, whereas Ube3a-as ASO does not. **(C)** Similar to **(B)**, but for ASO injection into adult mice. Neither Ube3a-as nor Snord115 reduces poly-spikes. The numbers of tested mice are indicated in the figure. Each filled (male) or open (female) circle represents one mouse. Bar graphs are mean  $\pm$  standard error of the mean (SEM). Kruskal–Wallis test with Dunn's multiple comparison test for all pairs of groups, \* $p$  < 0.05, \*\* $p$  < 0.01, \*\*\* $p$  < 0.001, \*\*\*\* $p$  < 0.0001.

The online version of this article includes the following figure supplement(s) for figure 7:

**Figure supplement 1.** Poly-spikes in the somatosensory and visual cortices of *Ube3a*<sup>Δe6/p+</sup> mice.

## Modulation of EEG rhythms and REM sleep by ASOs tracks the *Ube3a* protein levels in *Ube3a*<sup>Δe6/p+</sup> mice

Our results above show that Ube3a-as ASO and Snord115 ASO upregulate Ube3a proteins (**Figure 3**; **Figure 3—figure supplement 2**) and modulate EEG rhythms (**Figure 5**) and REM sleep (**Figure 6**) to different extents in *Ube3a*<sup>Δe6/p+</sup> mice depending on the age of ASO injection and post injection time. To understand how well the modulation of EEG rhythms and REM sleep by the ASOs reflects the Ube3a protein levels, we determined the relationships between Ube3a protein levels and EEG relative power in different frequency bands, power ratio ( $\alpha + \beta_1 + \beta_2$ )/ $\gamma_2$ , or time in REM sleep. We first averaged the Ube3a protein levels across different brain regions to estimate the overall Ube3a protein levels in each mouse from the Western blot experiments (**Figure 3**; **Figure 3—figure supplement 2**) and then obtained the mean Ube3a protein levels at each of the 3-, 6-, and 10-week timepoints post ASO injection. Since the Ube3a protein levels in *Ube3a*<sup>Δe6/p+</sup> mice were expressed a fraction of the WT levels, for the corresponding EEG relative power in different frequency bands, power ratio ( $\alpha + \beta_1 + \beta_2$ )/ $\gamma_2$ , and time in REM sleep, we also normalized the data by the means of those in the corresponding control ASO-treated WT mice. For both ASO injection into juvenile and adult mice, the relative power in the theta ( $\theta$ , 4–8 Hz), alpha ( $\alpha$ , 8–13 Hz), low beta ( $\beta_1$ , 13–18 Hz), and high beta ( $\beta_2$ , 18–25 Hz) bands negatively correlated with the Ube3a protein levels, whereas the relative power in the low gamma ( $\gamma_1$ , 25–50 Hz) and high gamma ( $\gamma_2$ , 50–100 Hz) bands positively correlated with the Ube3a protein levels. Therefore, the power ratio ( $\alpha + \beta_1 + \beta_2$ )/ $\gamma_2$  also negatively correlated with the Ube3a protein levels (**Figure 8A**). However, the relative power in the delta ( $\delta$ , 1–4 Hz) band did not correlate with the Ube3a protein levels (**Figure 8A**). Finally, the time in REM sleep during the light phase positively correlated with the Ube3a protein levels too (**Figure 8B**). In the dark phase, the positive correlation between the time in REM sleep and the Ube3a protein levels existed only for the ASO injection into the juvenile mice (**Figure 8B**). Hence, these results indicate that the relative power

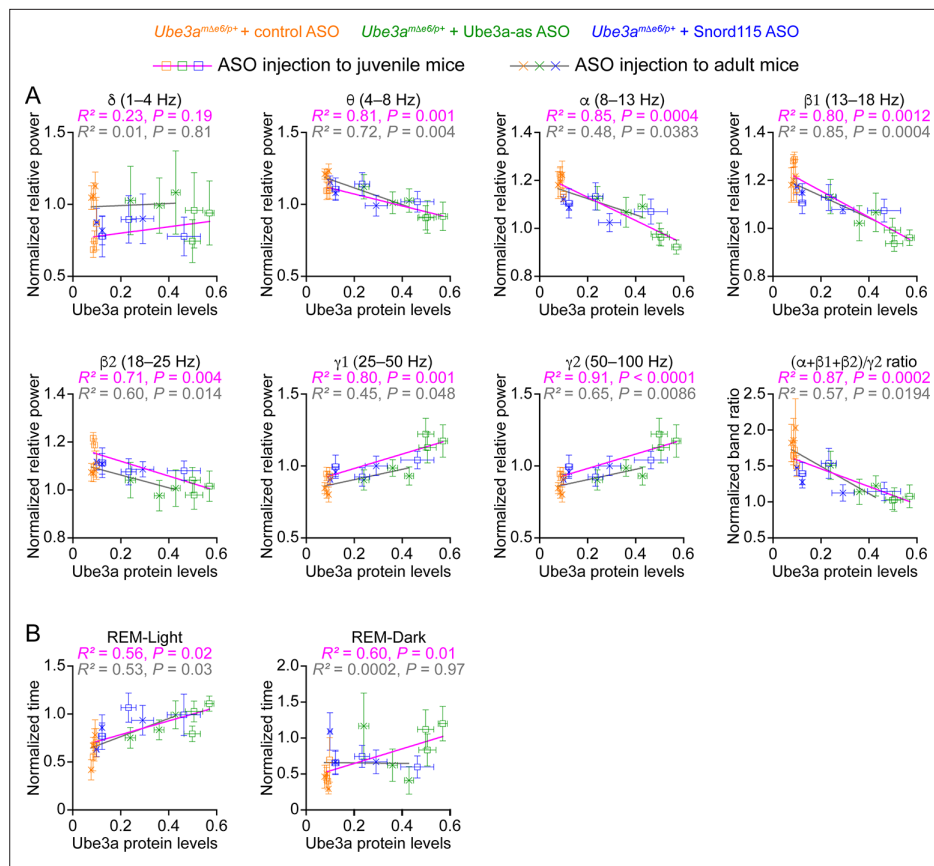


**Figure 8.** Electroencephalogram (EEG) rhythms and rapid eye movement (REM) sleep correlate with Ube3a protein levels in *Ube3a*<sup>Δe6/p+</sup> mice. **(A)** The relationships between the Ube3a protein levels and EEG relative power from the frontal cortices of *Ube3a*<sup>Δe6/p+</sup> mice injected with control, Ube3a-as, or Snord115 antisense oligonucleotide (ASO) across 3, 6, and 10 weeks post ASO injection into juvenile and adult mice. The Ube3a protein levels from all brain regions were averaged for each mouse. The relative EEG power within each frequency band and the power ratio ( $\alpha + \beta_1 + \beta_2$ )/ $\gamma_2$  were normalized by the means of those in wild-type (WT) mice injected with control ASO. The relationships were fitted with a linear regression ( $Y = aX + b$ ; X, Ube3a protein levels; Y, normalized EEG relative power or power ratio ( $\alpha + \beta_1 + \beta_2$ )/ $\gamma_2$ ; a, b, constants). **(B)** Similar to **(A)**, but for the relationships between the Ube3a protein levels and REM sleep time in light and dark phases. Data are mean  $\pm$  standard error of the mean (SEM).  $R^2$  indicates the goodness of fit.  $p < 0.05$  indicates a significant deviation of slope from zero.

of EEG rhythms and time in REM sleep dynamically follow the Ube3a protein levels in *Ube3a*<sup>Δe6/p+</sup> mice that are regulated by the ASOs.

## Discussion

Genetic approaches to restoring *UBE3A* expression holds great promise for treating Angelman syndrome because they tackle the disease root cause. Three active clinical trials of *UBE3A*-ATS-targeted ASOs have generated a great deal of excitement and expectation in the community. Meanwhile, an increasing number of studies in mouse models of Angelman syndrome demonstrate that Ube3a must be reinstated in late embryonic and early postnatal development to correct most neurological phenotypes (Silva-Santos et al., 2015; Gu et al., 2019; Rotaru et al., 2018; Sonzogni et al., 2020). Among the previously tested phenotypes, only a small subset (i.e., synaptic transmission, plasticity, and spatial memory) can be improved upon increasing Ube3a at the age of 6 weeks or older, and slightly a few more (i.e., rotarod performance and susceptibility to seizure induction) when increasing Ube3a at postnatal day 21 (Supplementary file 1). Despite limited prior successes in rescuing juvenile and adult maternal Ube3a deficiency mice, we chose these two ages to examine the effects of ASO therapy on

cortical hyperexcitability, altered EEG power spectrum, and sleep disturbance because these ages are more translationally relevant than the neonatal period. Our study reveals that a single ICV injection of *Ube3a*-ATS-targeted ASOs to *Ube3a<sup>mΔe6/p+</sup>* mice, a new rodent model of Angelman syndrome (*Shi et al., 2022*), upregulates *Ube3a* proteins including the critical short isoform and restores the EEG power spectrum and sleep pattern for at least 6 weeks, particularly upon treatment at the juvenile age. Therefore, our results significantly expand the range of phenotypes that can be reversed by restoring *Ube3a* expression in juvenile and adult mice. Interestingly, we were not able to reduce the frequency of poly-spikes in *Ube3a<sup>mΔe6/p+</sup>* mice at either age (*Figure 7*). It is possible that suppression of poly-spikes requires upregulation of *Ube3a* starting at a younger age or reaching to a higher level than what we have achieved, both of which should be tested in future studies. Nevertheless, this result indicates that poly-spikes are independent from the EEG power spectrum and sleep pattern deficits, and probably involve a different mechanism.

A critical finding of our study is that the improvement in the EEG power spectrum and sleep pattern tracks the increase in *Ube3a* protein levels across different ASOs, injection ages, and timepoints post injection (*Figure 8*). This suggests that following a bolus injection of ASOs, both phenotypes are acutely modulated by the *Ube3a* levels that decrease over time due to ASO clearance. Future studies should determine if repeated administration of ASOs can generate a long-lasting improvement of the phenotypes beyond the period when *Ube3a* levels are sufficiently upregulated, as the outcome can help inform the ASO treatment schedule in clinical trials. The ASO treatment in adult mice is less effective than juvenile mice, which is consistent with a recent finding that treating *Ube3a<sup>mΔe5/p+</sup>* mice with *Ube3a*-as ASO around P35 modestly reduced the EEG PSD in the delta frequency band (*Spencer et al., 2022*). This could be due to two reasons. First, the reversibility of disturbed EEG power spectrum and sleep may decrease over age, just like other neurological deficits (*Supplementary file 1*). Second, the ASO treatment in adult mice causes a smaller increase of *Ube3a* protein than juvenile mice (*Figure 3*). Given the strong correlation between *Ube3a* levels and phenotypic improvement, we speculate that the latter is more likely the reason, and a higher dose of ASO or an ASO with a higher efficacy in downregulating *Ube3a*-ATS should further increase *Ube3a* protein and improve these two phenotypes in adult mice.

Previous EEG studies of *Ube3a<sup>mΔe5/p+</sup>* mice emphasized an increase of absolute power or PSD in the delta frequency band as compared to WT mice, but the results varied among studies (*Ehlen et al., 2015; Born et al., 2017; Sidorov et al., 2017; Copping and Silverman, 2021*). One study recorded local field potential in layer 4 of the primary visual cortex from awake mice that were head-fixed and viewing a static gray screen. The absolute delta (2–4 Hz) power of local field potential was increased when *Ube3a<sup>mΔe5/p+</sup>* mice were on a 129 strain background, but not on a C57BL/6 background. Interestingly, a reduction of the relative power in the gamma band (30–50 Hz) was observed in both strains (*Sidorov et al., 2017*). In contrast, two other studies reported an increase in delta (0–4 or 0.5–4 Hz) power of chronic EEG recorded from the cortical surface of freely moving *Ube3a<sup>mΔe5/p+</sup>* mice on a C57BL/6 background (*Born et al., 2017; Copping and Silverman, 2021*), but not on a 129 strain background (*Born et al., 2017*). Finally, it was reported that the relative delta power of cortical surface EEG was reduced in *Ube3a<sup>mΔe5/p+</sup>* mice on the C57BL/6J background during NREM sleep in the night, but not in the day (*Ehlen et al., 2015*). Our absolute PSD results from the new *Ube3a<sup>mΔe6/p+</sup>* mice are qualitatively similar to the previous results (*Figure 5—figure supplement 1*), but relative PSD analysis reveals an increase of relative power in the theta, alpha, or beta frequency bands and a decrease in the low or high gamma frequency bands. These differences could be due to different mutations, genetic backgrounds, mouse ages, experimental conditions, or different brain states included in the analyses. Nevertheless, we observed a robust and consistent increase in the power ratio ( $\alpha + \beta_1 + \beta_2$ )/ $\gamma_2$  across timepoints (*Figure 5*). In fact, inspection of previous results suggests a common pattern that EEG power is relatively higher in maternal *Ube3a* deficiency mice than WT mice in the lower frequency bands (i.e., beta or lower) and relatively lower in the gamma bands, although the results were not always statistically significant (*Born et al., 2017; Sidorov et al., 2017; Copping and Silverman, 2021*). Similarly, the EEG power spectrum of Angelman syndrome patients also shows such a pattern (*Sidorov et al., 2017*). Thus, we propose that a power ratio between the low- and high-frequency bands would be a more robust measure of the EEG power spectrum phenotype in Angelman syndrome and its mouse models.

The EEG power spectrum and sleep phenotypes of maternal *Ube3a* knockout mice directly correlate with those in Angelman syndrome patients, but about 70% of Angelman syndrome patients have a larger deletion in the chromosomal region 15q11–q13 that encompasses *UBE3A* and other genes with biallelic or paternal expression (Bird, 2014; Buiting et al., 2016). These deletion Angelman syndrome patients have more severe clinical phenotypes (Williams et al., 2006; Bird, 2014; Buiting et al., 2016) and a larger increase in the EEG theta band power (Frohlich et al., 2019) than non-deletion patients, suggesting that the heterozygosity of those biallelically expressed genes contribute to the severity of Angelman syndrome. Thus, future studies are necessary to determine the contribution of these genes to the neurological phenotypes including disturbed EEG power spectrum and sleep. Particularly, the *GABRB3*, *GABRA5*, and *GABRG3* genes in this region encode GABA<sub>A</sub> receptor subunit β3, α5, and γ3, respectively, and are likely to be critical given the vital role of GABAergic inhibition in brain functions and the fact that heterozygous loss-of-function *GABRB3* variants cause a broad spectrum of epilepsies (Møller et al., 2017). The *HERC2* gene encoding HECT domain and RCC1-like domain 2 can also be important because this E3 ubiquitin protein ligase interacts with *UBE3A* (Kühnle et al., 2011) and its loss-of-function causes a neurodevelopmental disorder with Angelman syndrome-like features (Puffenberger et al., 2012; Harlalka et al., 2013). Since *UBE3A*-ATS-targeted ASOs do not affect these biallelically expressed genes, it will be of great importance to determine to what extent reactivating paternal *Ube3a* can rescue the EEG power spectrum and sleep phenotypes in a large deletion mouse model (Jiang et al., 2010).

Our study has several translational implications for the ASO and other clinical trials of Angelman syndrome. First, even though it is unclear how the mouse developmental stages in which the neurological phenotypes can be reversed are related to the treatment window for Angelman syndrome, our results suggest that Angelman syndrome patients at different ages may all benefit from the ASO treatment of these two core disease symptoms. Second, the robust correlation between EEG power spectrum and *Ube3a* levels supports the notion that EEG power spectrum can serve as a quantitative biomarker in clinical trials (Sidorov et al., 2017; Frohlich et al., 2019; Hipp et al., 2021; Ostrowski et al., 2021). Third, since the EEG power of Angelman syndrome patients correlates with their symptom severity, particularly the cognitive function (Hipp et al., 2021; Ostrowski et al., 2021), it is reasonable to speculate that ASO treatment may also improve the cognitive function of Angelman syndrome patients. Finally, clinicians and caregivers consider sleep disturbance as one of the most challenging symptoms and important focuses for new treatment (Willgoss et al., 2021). Thus, if ASO therapy can reduce sleep disturbance, then it will improve quality of life for both Angelman syndrome patients and caregivers.

## Materials and methods

### Key resources table

Reagent type (species) or resource	Designation	Source or reference	Identifiers	Additional information
Genetic reagent ( <i>Mus musculus</i> )	<i>Ube3a</i> <sup>Δe6</sup>	This paper		The new <i>Ube3a</i> KO allele that deletes exon 6
Genetic reagent ( <i>Mus musculus</i> )	B6.129S7- <i>Ube3a</i> <sup>tm1Aib</sup> /J	The Jackson Laboratory	RRID:IMSR_JAX:016590	The previous <i>Ube3a</i> KO allele that deletes exon 5, <i>Ube3a</i> <sup>Δe5</sup> in the paper
Genetic reagent ( <i>Mus musculus</i> )	B6.129S7- <i>Ube3a</i> <sup>tm2Aib</sup> /J	The Jackson Laboratory	RRID:IMSR_JAX:017765	<i>Ube3a</i> <sup>YFP</sup> in the paper
Genetic reagent ( <i>Mus musculus</i> )	C57BL/6J	The Jackson Laboratory	RRID:IMSR_JAX:000664	
Sequence-based reagent	Control ASO	Ionis Pharmaceuticals, <a href="#">Meng et al., 2015</a>		5'-CCToAoToAoGGACTATCCAoGoGAA-3'
Sequence-based reagent	<i>Ube3a</i> -as ASO	Ionis Pharmaceuticals, <a href="#">Meng et al., 2015</a>		5'-CCoAoGoCoCTTGTGGATAoToCAT-3'
Sequence-based reagent	Snord115 ASO	Ionis Pharmaceuticals, this paper		5'-TToGoToAoAGCATCAAAGToAoTGA-3'

Continued on next page

Continued

Reagent type (species) or resource	Designation	Source or reference	Identifiers	Additional information
Antibody	Rabbit monoclonal anti-GFP	Invitrogen	Cat. #: G10362	IF (1:2000)
Antibody	Mouse monoclonal anti-E6AP	Sigma-Aldrich	Cat. #: E8655	WB (1:1000)
Antibody	Mouse monoclonal anti-Gapdh	Proteintech	Cat. #: 60004-1-Ig	WB (1:10,000)
Antibody	Mouse monoclonal anti-β3 tubulin	Proteintech	Cat. #: 66240-1-Ig	WB (1:50,000)
Antibody	Goat polyclonal anti-rabbit secondary antibody conjugated with Alexa Flour 647	Invitrogen	Cat. #: A21245	IF (1:1000)
Antibody	Goat polyclonal anti-mouse antibody conjugated with IRDye 800CW	LI-COR Bioscience	Cat. #: 925-32210	WB (1:20,000)
Other	NeuroTrace 435/455 blue fluorescent Nissl stain	Invitrogen	Cat. #: N21479	IF (1:200)
Other	Bolt Bis-Tris Plus 10% mini protein gels	Thermo Fisher Scientific	Cat. #: NW00107BOX	SDS-PAGE for total Ube3a
Other	Novex Tris-Glycine 4–12% mini protein gels	Thermo Fisher Scientific	Cat. #: XP04120BOX	SDS-PAGE for separation of Ube3a isoforms
Software, algorithm	LAS X software	Leica	RRID: <a href="#">SCR_013673</a>	Version 3.3.0.16799
Software, algorithm	ImageJ	NIH	RRID: <a href="#">SCR_003070</a>	Version 1.53c
Software, algorithm	LABKIT	<b>Arzt et al., 2022</b>		Version 0.3.9, <a href="https://imagej.net/plugins/labkit/">https://imagej.net/plugins/labkit/</a>
Software, algorithm	Image Studio Lite	LI-COR Biosciences	RRID: <a href="#">SCR_013715</a>	Version 5.2
Software, algorithm	Sirenia	Pinnacle Technology	RRID: <a href="#">SCR_016184</a>	Version 1.8.2
Software, algorithm	SPINDLE	<b>Miladinović et al., 2019</b>		<a href="https://sleeplearning.ethz.ch">https://sleeplearning.ethz.ch</a>
Software, algorithm	Prism	GraphPad Software	RRID: <a href="#">SCR_002798</a>	Version 9
Software, algorithm	Python	Python Software Foundation	RRID: <a href="#">SCR_008394</a>	Version 3.9.12

## Mice

The new *Ube3a* null allele was generated by CRISPR/Cas9-mediated deletion of exon 6. WT Cas9 mRNA (100 ng/μl) and two sgRNAs (10 ng/μl each) targeting the genomic sequences of *Ube3a* intron 5 (5'-TTACATACCAGTACATGTCTTG-3') and intron 6 (5'-TGCTTCTACCAACTGAGACAGG-3') were microinjected into WT C57BL/6J (JAX # 000664) zygotes. Founder mice carrying the exon 6 deletion (*Ube3a*<sup>Δe6</sup>) were identified by PCR using a pair of primers (5'-TTGAGAACATGCAAAGGAAAATGA-3' and 5'-GAGCAAAGTGTAGACCC-3') for the WT allele (747 bp) and a pair of primers (5'-TTGA GAACAATGCAAAGGAAAATGA-3' and 5'-TGAGGGCTGGCTTCAAGATTCA-3') for the Δe6 (314 bp) allele. Founder mice were then backcrossed to WT C57BL/6J mice to generate N1 mice. N1 mice carrying the Δe6 allele were identified using the same PCR above. Sequencing of the identified N1 mice confirmed that the sequence chr7:59,275,513–59,277,423 were deleted. *Ube3a*<sup>Δe6</sup> mice were

backcrossed to WT C57BL/6J mice for at least five generations prior to experiments. Heterozygous female mice carrying the mutation on their paternal chromosome (*Ube3a*<sup>m+/pΔe6</sup>) were crossed with WT C57BL/6J mice to generate WT and maternal knockout of *Ube3a* mice (*Ube3a*<sup>mΔe6/p+</sup>).

*Ube3a*<sup>Δe5</sup> mice (*Ube3a*<sup>tm1Alb</sup>, JAX # 016590) were described previously (Jiang et al., 1998), in which exon 5 was deleted. Heterozygous female *Ube3a*<sup>m+/pΔe5</sup> mice were crossed with WT C57BL/6J mice to generate WT and *Ube3a*<sup>mΔe5/p+</sup> mice. Heterozygous male and female *Ube3a*<sup>m+/pΔe5</sup> mice were crossed with each other to generate WT and *Ube3a*<sup>mΔe5/mΔe5</sup> mice. *Ube3a*<sup>YFP</sup> mice (*Ube3a*<sup>tm2Alb</sup>, JAX #017765) were described previously (Dindot et al., 2008) and carry a *Ube3a* knockin allele with a yellow fluorescent protein (YFP) fused to the C terminus of *Ube3a*. Heterozygous male or female *Ube3a*<sup>m+/pYFP</sup> mice were crossed with WT C57BL/6J mice to obtain heterozygous paternal or maternal *Ube3a*<sup>YFP</sup> mice (*Ube3a*<sup>m+/pYFP</sup> or *Ube3a*<sup>mYFP/p+</sup>), respectively. *Ube3a*<sup>Δe5</sup> and *Ube3a*<sup>YFP</sup> mice were also maintained on the C57BL/6J background.

Mice were housed in an Association for Assessment and Accreditation of Laboratory Animal Care International-certified animal facility on a 14/10 hr light/dark cycle. All procedures to maintain and use mice were performed in strict accordance with the recommendations in the Guide for the Care and Use of Laboratory Animals of the National Institutes of Health and were approved by the Institutional Animal Care and Use Committee at Baylor College of Medicine (protocol AN-6544).

### Reverse transcription droplet digital PCR

Mice were anesthetized and decapitated. Brain and liver tissues were extracted and homogenized with Trizol (Thermo Fisher, catalog #15596026), followed by RNase-free DNase treatment (Qiagen, catalog #79254). RNAs were purified with RNeasy Plus Mini Kit (Qiagen, catalog #74136) and reverse transcribed to cDNA by High-Capacity cDNA Reverse Transcription Kit (Thermo Fisher, catalog #4368814). The cDNA concentration was determined by a Nanodrop (Thermo Fisher). Droplet digital PCR (ddPCR) was prepared by mixing the following reagents in a total volume of 20  $\mu$ l: 2x QX200 ddPCR EvaGreen supermix (Bio-Rad, catalog #1864036, 10  $\mu$ l), forward and reverse primers (10  $\mu$ M, 0.4  $\mu$ l each), cDNA template (10–100 ng, 1  $\mu$ l), and nuclease-free H<sub>2</sub>O (8.2  $\mu$ l). The droplets for ddPCR were generated by a Biorad Automated Droplet Generator (Bio-Rad, catalog #1864101), followed by PCR reaction using a Thermal Cycler C1000 (Bio-Rad). The plate containing the droplets was read by a QX200 Droplet reader (Bio-Rad, catalog #1864001). The primers for detecting different fragments of the *Ube3a* transcripts are provided in **Supplementary file 2**. The expression levels of *Ube3a* transcripts were normalized by the *Gapdh* levels.

### Antisense oligonucleotides

Synthesis and purification of all chemically modified oligonucleotides were performed as previously described (Swayze et al., 2007). The 2'-O-methoxyethylribose (MOE) gapmer ASOs are 20 nucleotides in length, wherein the central gap segment comprising ten 2'-deoxynucleotides is flanked on the 5' and 3' wings by five 2'-MOE modified nucleotides. All internucleoside linkages are phosphorothioate linkages, except the ones shown as 'o' in the sequences which are phosphodiester. The sequences of the ASOs are as follows: control ASO, 5'-CCToAoToAoGGACTATCCAOGoGAA-3'; *Ube3a*-as ASO, 5'-CCoAoGoCoCTTGTTGGATAoToCAT-3'; and Snord115 ASO, 5'-TToGoToAoAGCATCAAAGToAoT GA-3'. Lyophilized ASOs were formulated in phosphate-buffered saline (PBS) without Ca<sup>2+</sup> and Mg<sup>2+</sup> (Gibco, catalog # 14190). ASOs were dissolved in PBS to obtain 50 mg/ml concentrations.

### ICV injection of ASOs

Mice were anesthetized with isoflurane (1.5–2.5%) in oxygen (1 l/min). The body temperature was monitored and maintained at 37°C using a temperature controller (ATC-2000, World Precision Instruments). An incision was made along the midline to expose the skull after the head was fixed in a stereotaxic apparatus. Approximately 0.25-mm-diameter craniotomies were performed with a round bur (0.25-mm-diameter) and a high-speed rotary micromotor (EXL-M40, Osada) at the injection site (see below). A bevelled 50- $\mu$ m-diameter glass pipette was used to inject ASOs into the right lateral ventricle according to one of the following sets of coordinates that were normalized by the distance between Bregma and Lambda (DBL). (1) Anterior/posterior (AP): 0.055 of DBL, medial/lateral (ML): 0.238 of DBL, dorsal/ventral (DV): -0.499 of DBL; (2) AP: 0.055 of DBL, ML: 0.238 of DBL, DV: -0.594

of DBL; (3) AP: 0.071 of DBL, ML: 0.238 of DBL, DV, -0.713 of DBL. The results were similar among these three sets of coordinates and were grouped together. ASO solution was injected at a rate of 407 nl/s using an UltraMicroPump III and a Micro4 controller (VAR-3735, World Precision Instruments). A total of 10  $\mu$ l ASO solution (50 mg/ml) was administered for a total dosage of 500  $\mu$ g/mouse except six mice that were injected with 5  $\mu$ l ASO solution for a total dosage of 250  $\mu$ g/mouse at the age of 3 weeks and used in the Western blot experiments. The results from these six mice were similar to other mice (**Figure 3—figure supplement 5**) and grouped together. After injection, the pipette was held in place for 10 min before withdrawal. The skin was sutured, and mice were allowed to recover from anesthesia in a cage placed on a heating pad. When the recovery takes longer than 1 hr, the duration on the heating pad should not exceed 1 hr, as longer exposure of mice on the heating pad significantly reduces post-surgery survival rates (less than 1 hr: 1 out of 102 injected mice died, more than 1 hr: 31 out of 106 injected mice died,  $p < 0.0001$ ).

### Immunohistochemistry and fluorescent microscopy

Mice were anesthetized and transcardially perfused with PBS (pH 7.4) followed by 4% paraformaldehyde in PBS (pH 7.4). Brains were then post-fixed for overnight in 4% paraformaldehyde at 4°C and sectioned into 40- $\mu$ m sagittal slices using a vibratome (VT1000S, Leica). Brain sections were incubated in blocking solution (0.2% Triton X-100 in PBS with 5% normal goat serum) for 1 hr at 4°C and then with a primary rabbit monoclonal anti-GFP antibody (Invitrogen, catalog # G10362, lot # 1965886, 1:2000 dilution) that recognizes YFP for overnight at 4°C. Sections were washed with 0.2% Triton X-100 in PBS and then incubated with a goat polyclonal anti-rabbit secondary antibody conjugated with Alexa Flour 647 (Invitrogen, catalog # A21245, lot # 1623067, 1:1000 dilution) in blocking solution for 3 hr at room temperature. After antibody staining, sections were incubated with NeuroTrace 435/455 blue fluorescent Nissl stain (Invitrogen, catalog # N21479, 1:200 dilution) in 0.2% Triton X-100 in PBS at room temperature for 1 hr to label neurons. Sections were washed with 0.2% Triton X-100 in PBS and mounted in ProLong Diamond Antifade Mountant (Invitrogen, catalog # P36961). High-resolution (1024  $\times$  1024) single-plane images of the brain sections were acquired on a TCS SP8X Confocal Microscope (Leica) using a  $\times$ 20 oil objective (HC PL APO CS2  $\times$ 20, NA = 0.75). Mosaic images were stitched together using LAS X software v3.3.0.16799 (Leica) and visualized and exported by ImageJ 1.53c (NIH). To quantify Ube3a-YFP levels, cell somas were identified and segmented based on fluorescent Nissl stain using an ImageJ plugin, LABKIT (Arzt et al., 2022). For each image, YFP fluorescence intensity was measured and averaged across all identified cell somas and then normalized by the mean of *Ube3a*<sup>mYFP/+</sup> mice.

### Western blot and RT-qPCR

Mice were anesthetized and decapitated. The brains were extracted, and different regions were dissected from both hemispheres. The brain tissues from the right hemisphere were used for Western blots and the left hemisphere for RT-qPCR. Tissues were frozen at -80°C until analysis.

For Western blots, the brain tissues were homogenized in RIPA buffer containing 50 mM Tris-HCl (pH 8.0), 150 mM NaCl, 1% Triton X-100, 0.5% Na-deoxycholate, 0.1% sodium dodecyl sulfate (SDS), 1 mM ethylenediaminetetraacetic acid (EDTA), 5% glycerol, and 1 cOmplete Protease Inhibitor tablet (Roche, # SKU 11836170001). After homogenization, tissue debris was removed by centrifugation and protein concentrations were determined by Pierce BCA Protein Assay Kit (Thermo Fisher Scientific, catalog # 23225). To measure total Ube3a, 10  $\mu$ g of proteins per sample were resolved by SDS-polyacrylamide gel electrophoresis (PAGE) with 10% Bis-Tris gels (Thermo Fisher Scientific, catalog # NW00107BOX) and transferred onto nitrocellulose membranes. To separate the two Ube3a isoforms, 3  $\mu$ g of proteins per sample were resolved by SDS-PAGE with 4–12% Tris-Glycine gradient gels (Thermo Fisher Scientific, catalog # XP04120BOX) at 200 volts for 90 min. Ube3a was detected by a mouse monoclonal anti-E6AP antibody (Sigma-Aldrich, catalog # E8655, lot # 118M4792V, 1:1000 dilution) that recognizes both Ube3a isoforms 2 and 3. Gapdh was detected by a mouse monoclonal anti-Gapdh antibody (Proteintech, catalog # 60004-1-Ig, lot # 10004129, 1:10,000 dilution).  $\beta$ 3 tubulin was detected by a mouse monoclonal anti- $\beta$ 3 tubulin antibody (Proteintech, catalog # 66240-1-Ig, lot # 10004491, 1:50,000 dilution). Primary antibodies were detected by a goat polyclonal anti-mouse antibody conjugated with IRDye 800CW (LI-COR Bioscience, catalog # 925-32210, lot # C90130-03, 1:20,000 dilution). Proteins were visualized and

quantified using an Odyssey CLx Imager and Image Studio Lite version 5.2 (LI-COR Biosciences). To quantify the total Ube3a levels, both Ube3a isoforms 2 and 3 were included. To quantify the levels of each isoform, total Ube3a and isoform 3 were quantified, and the isoform 2 levels were measured by subtracting the isoform 3 levels from the total Ube3a levels. Total Ube3a, Ube3a isoform 2, or Ube3a isoform 3 levels were first normalized by the Gapdh or  $\beta$ 3 tubulin levels and then by the average total Ube3a, Ube3a isoform 2, or Ube3a isoform 3 of all WT mice from the same blot, respectively.

For RT-qPCR, the brain tissues were homogenized in RLT buffer (Qiagen, catalog # 79216) containing 1% (vol/vol)  $\beta$ -mercaptoethanol. Homogenization was performed for 20 s at 6000 rpm using a Fast-Prep Automated Homogenizer (MP Biomedicals). Total RNA was then purified using the RNeasy 96 Kit (Qiagen, catalog # 74182) that included an in-column DNA digestion with 50 U of DNase I (Invitrogen, catalog # 18047019). RT-qPCR was performed in triplicate with the EXPRESSS One-Step SuperScript qRT-PCR kit (Thermo Fisher Scientific, catalog # 11781200). Gene-specific primers and probes are provided in **Supplementary file 2**. The expression levels of Ube3a or Ube3a-ATS were normalized by the Gapdh levels and then by the average Ube3a or Ube3a-ATS levels of all WT mice from the same experiment, respectively.

## Video-EEG and EMG recordings

Video-EEG/EMG recordings were performed as previously described (Chen et al., 2020). Briefly, 1 week after ASO injection, mice were anesthetized with 2.5% isoflurane in oxygen, and craniotomies were performed as described above for ICV injection. Perfluoroalkoxy polymer (PFA)-coated silver wire electrodes (A-M Systems, catalog # 786000, 127 mm bare diameter, 177.8 mm coated diameter) were used for grounding at the right frontal cortex, referencing at the cerebellum, and recording at the left frontal cortex (AP: 0.475 of DBL, ML: -0.071 of DBL, DV: -1.5 mm), left somatosensory cortex (AP: -0.190 of DBL, ML: -0.428 of DBL, DV: -1.5 mm), and right visual cortex (AP: -0.808 of DBL, ML: 0.594 of DBL, DV: -1.5 mm). An EMG recording and an EMG reference electrode were inserted into the neck muscles. All electrodes were soldered to an adaptor prior to the surgery. The electrodes and adaptor were secured on the skull by dental acrylic. The skin was sutured and attached to the dried dental acrylic. Mice were singly housed to recover for at least 1 week after the surgeries. Before recording, mice were individually habituated in the recording chambers (10-inch diameter of Plexiglas cylinder) for 24 hr. EEG/EMG signals (5000 Hz sampling rate with a 0.5 Hz high-pass filter) and videos (30 frames/s) were recorded synchronously for more than 48 continuous hours using a 4-channel EEG/EMG tethered system and Sirenia 1.8.2 software (Pinnacle Technology).

## EEG poly-spikes and power spectrum analyses

Poly-spikes and PSD were analyzed from the same 6 hr of each recording (12 AM–1 AM, 4 AM–5 AM, 8 AM–9 AM, 12 PM–1 PM, 4 PM–5 PM, and 8 PM–9 PM on the second day). EEG/EMG traces were visualized in Sirenia Seizure 1.8.2 software (Pinnacle Technology) to identify episodes of poly-spikes and artifacts. An episode of poly-spikes is defined as a cluster of three or more spikes on any of the EEG channels. PSD analyses of EEG data were performed using custom scripts in Python. Prior to PSD calculation, data were detrended by subtracting the mean of the data. The data segments containing artifacts on any of the EEG channels were first excluded, and then an eighth-order Butterworth filter was applied to each channel to bidirectionally notch filter around 60 Hz ( $\pm 2$  Hz bandwidth) to remove power-line noise. The PSDs were then estimated for each channel using a Welch's periodogram (Welch, 1967) with a 2 s Hanning window (achieving a frequency resolution of 0.5 Hz) and 50% overlap between windows. To account for the effect of notch filtering, the PSD was linearly interpolated between 58 and 62 Hz using the 10 points before and after the mentioned ranges. To analyze different frequency bands, the PSD was segmented into seven bands: delta (1–4 Hz), theta (4–8 Hz), alpha (8–13 Hz), low beta (13–18 Hz), high beta (18–25 Hz), low gamma (25–50 Hz), and high gamma (50–100 Hz). The power within a frequency band (the area under the PSD curve for a band) was then computed for each band. The relative power in a frequency band is the ratio of the power within the band over the total power within 1–100 Hz. The normalized PSD curves were obtained by dividing the PSD curves with the total power within 1–100 Hz. The low- to high-frequency band ratio

was calculated as the ratio of the total power in the alpha and beta bands (8–25 Hz) over the power in the high gamma band (50–100 Hz).

## Sleep scoring

A convolutional neural network-based algorithm SPINDLE (<https://sleeplearning.ethz.ch>) was used for automated sleep scoring (Miladinović et al., 2019). This method produces domain invariant predictions and makes use of a hidden Markov model to limit state dynamics based on known sleep physiology. Sleep was scored from the entire second day (24 hr) of each recording. EEG signals from the frontal and somatosensory cortices and the EMG signals were used to score each 4 s epoch as wake, NREM sleep, or REM sleep. To assess the performance of this method on our dataset, two WT mice treated with control ASO, two *Ube3a<sup>mΔe6/p+</sup>* mice with control ASO, and one *Ube3a<sup>mΔe6/p+</sup>* mouse with *Ube3a-as* ASO were randomly selected and 1 hr of data from each mouse were scored by SPINDLE and manually by three experts. The Precision, Recall, *F*1-score, and Accuracy were calculated for each pairwise comparison as the following:  $Precision = \frac{\text{True positive}}{\text{True positive} + \text{False positive}}$ ;  $Recall = \frac{\text{True positive}}{\text{True positive} + \text{False negative}}$ ;  $F1\text{score} = 2 \times \frac{\text{Precision} \times \text{Recall}}{\text{Precision} + \text{Recall}}$ ;  $Accuracy = \frac{\text{True positive} + \text{True negative}}{\text{True positive} + \text{True negative} + \text{False positive} + \text{False negative}}$ . The accuracy of SPINDLE compared to experts was similar to that of the experts compared among each other (Figure 6—figure supplement 1).

## Experimental study design and statistics

Estimation of the sample size was made based on previous studies that used similar assays and pilot experiments. They are within the range that is generally accepted in the field. All experiments were performed and analyzed blind to the genotypes and ASOs. *Ube3a<sup>mΔe6/p+</sup>* mice were randomly assigned to three groups, each of which received control, *Ube3a-as*, or Snord115 ASO. Approximately equal number of male and female mice was included in experiments. No data point was excluded.

All reported sample numbers (*n*) represent independent biological replicates that are the numbers of tested mice. Statistical analyses were performed with Prism 9 (GraphPad Software). Student's *t*-test or analysis of variance (ANOVA) with multiple comparison test for all pairs of groups was used to determine if there is a statistically significant difference between two groups or among three or more groups, respectively. One- or two-way ANOVA was applied for one or two independent variables, respectively. Anderson–Darling test, D'Agostino–Pearson, Shapiro–Wilk, and Kolmogorov–Smirnov tests were used to determine if data were normally distributed. Non-parametric Kruskal–Wallis one-way ANOVA with Dunn's multiple comparison test was used for low- to high-frequency band ratio and poly-spike data. The details of all statistical tests, numbers of replicates, and *p* values are reported in Supplementary file 3.

## Materials, data, and code availability

Following the material transfer agreement of Baylor College of Medicine, *Ube3a<sup>Δe6</sup>* mice will be available upon request or from the Jackson Laboratory (JAX). All data generated or analyzed during this study are included in the manuscript. Computer codes for EEG power spectrum analyses and sleep scoring are available at GitHub (<https://github.com/heetkaku/angelman>, copy archived at <https://zenodo.org/record/5812234>, Kaku, 2022).

## Acknowledgements

We thank Jacob, Debra, and Steven Sukin for inspiring this work, Baylor College of Medicine Genetically Engineered Rodent Models Core led by Dr. Jason Heaney for microinjection of Cas9 mRNA and sgRNAs to generate *Ube3a<sup>Δe6</sup>* mice, and Drs. Catherine Chu, Robert Komorowski, James Gilbert, Rodney Samaco, and Huda Zoghbi for discussions. This work was supported in part by the Main Street America Fund at Texas Children's Hospital, the Eunice Kennedy Shriver National Institute of Child Health and Human Development (P50HD103555 to Baylor College of Medicine Intellectual and Developmental Disabilities Research Center, Neurovisualization Core), and the National Cancer Institute (P30CA125123 to Baylor College of Medicine Cancer Center). MX was supported by the National Institute of Neurological Disorders and Stroke (R01NS100893) and the National Institute of Mental Health (R01MH117089) and is a Caroline DeLuca Scholar.

## Additional information

### Competing interests

Armand Soriano, Frank Rigo, Paymaan Jafar-nejad: is a paid employee of Ionis Pharmaceuticals. Arthur L Beaudet: is a paid employee of Luna Genetics. Mingshan Xue: is a consultant to Capsida Biotherapeutics and receives funds from Capsida Biotherapeutics for research not related to this study. The other authors declare that no competing interests exist.

### Funding

Funder	Grant reference number	Author
Texas Children's Hospital	Main Street America Fund	Mingshan Xue
National Institute of Neurological Disorders and Stroke	R01NS100893	Mingshan Xue
National Institute of Mental Health	R01MH117089	Mingshan Xue

The funders had no role in study design, data collection, and interpretation, or the decision to submit the work for publication.

### Author contributions

Dongwon Lee, Data curation, Formal analysis, Investigation, Visualization, Methodology, Writing – original draft, Writing – review and editing; Wu Chen, Data curation, Formal analysis, Supervision, Investigation, Visualization, Methodology, Writing – original draft, Writing – review and editing; Heet Naresh Kaku, Data curation, Software, Formal analysis, Investigation, Visualization, Methodology, Writing – original draft, Writing – review and editing; Xinming Zhuo, Eugene S Chao, Formal analysis, Investigation, Methodology, Writing – review and editing; Armand Soriano, Allen Kuncheria, Stephanie Flores, Joo Hyun Kim, Investigation, Writing – review and editing; Armando Rivera, Investigation, Methodology, Writing – review and editing; Frank Rigo, Supervision, Writing – review and editing; Paymaan Jafar-nejad, Supervision, Methodology, Writing – review and editing; Arthur L Beaudet, Conceptualization, Supervision, Writing – review and editing; Matthew S Caudill, Software, Supervision, Methodology, Writing – review and editing; Mingshan Xue, Conceptualization, Supervision, Funding acquisition, Visualization, Methodology, Writing – original draft, Project administration, Writing – review and editing

### Author ORCIDs

Wu Chen  <http://orcid.org/0000-0002-7400-0519>  
Armando Rivera  <http://orcid.org/0000-0001-7076-8566>  
Mingshan Xue  <http://orcid.org/0000-0003-1463-8884>

### Ethics

This study was performed in strict accordance with the recommendations in the Guide for the Care and Use of Laboratory Animals of the National Institutes of Health. All of the animals were handled according to approved Institutional Animal Care and Use Committee (IACUC) protocols (AN-6544) of Baylor College of Medicine.

### Decision letter and Author response

Decision letter <https://doi.org/10.7554/eLife.81892.sa1>  
Author response <https://doi.org/10.7554/eLife.81892.sa2>

## Additional files

### Supplementary files

- Supplementary file 1. Comparison of phenotypic rescue of maternal *Ube3a* knockout mice by restoring *Ube3a* expression at different ages. The table summarizes the outcomes of restoring *Ube3a* expression in maternal *Ube3a* knockout mice at different developmental ages from previous studies.

- Supplementary file 2. Primers and probes for reverse transcription droplet digital PCR (RT-ddPCR) and reverse transcription quantitative real-time PCR (RT-qPCR). The sequences of the primers and probes used in the RT-ddPCR or RT-qPCR experiments for detecting *Ube3a*, *Ube3a-ATS*, *Ipw*, and *Gapdh* are provided.
- Supplementary file 3. Statistics of experimental results. The details of all statistical tests, numbers of replicates, and p values are presented for each experiment in the table.
- MDAR checklist

#### Data availability

All data generated or analyzed during this study are included in the manuscript and supporting file; Source Data files have been provided for Figure 3, Figure 3-supplement 1, Figure 3-supplement 3, and Figure 3-supplement 4.

## References

- Albrecht U**, Sutcliffe JS, Cattanach BM, Beechey CV, Armstrong D, Eichele G, Beaudet AL. 1997. Imprinted expression of the murine Angelman syndrome gene, *Ube3a*, in hippocampal and Purkinje neurons. *Nature Genetics* **17**:75–78. DOI: <https://doi.org/10.1038/ng0997-75>, PMID: 9288101
- Arzt M**, Deschamps J, Schmied C, Pietzsch T, Schmidt D, Tomancak P, Haase R, Jug F. 2022. LABKIT: labeling and segmentation toolkit for big image data. *Frontiers in Computer Science* **4**:777728. DOI: <https://doi.org/10.3389/fcomp.2022.777728>
- Avagliano Trezza R**, Sonzogni M, Bossuyt SNV, Zampeta FI, Punt AM, van den Berg M, Rotaru DC, Koene LMC, Munshi ST, Stedehouder J, Kros JM, Williams M, Heussler H, de Vrij FMS, Mientjes EJ, van Woerden GM, Kushner SA, Distel B, Elgersma Y. 2019. Loss of nuclear *Ube3a* causes electrophysiological and behavioral deficits in mice and is associated with Angelman syndrome. *Nature Neuroscience* **22**:1235–1247. DOI: <https://doi.org/10.1038/s41593-019-0425-0>, PMID: 31235931
- Bird LM**. 2014. Angelman syndrome: review of clinical and molecular aspects. *The Application of Clinical Genetics* **7**:93–104. DOI: <https://doi.org/10.2147/TACG.S57386>, PMID: 24876791
- Born HA**, Dao AT, Levine AT, Lee WL, Mehta NM, Mehra S, Weeber EJ, Anderson AE. 2017. Strain-dependence of the angelman syndrome phenotypes in UBE3A maternal deficiency mice. *Scientific Reports* **7**:8451. DOI: <https://doi.org/10.1038/s41598-017-08825-x>, PMID: 28814801
- Born HA**, Martinez LA, Levine AT, Harris SE, Mehra S, Lee WL, Dindot SV, Nash KR, Silverman JL, Segal DJ, Weeber EJ, Anderson AE. 2021. Early developmental EEG and seizure phenotypes in a full gene deletion of ubiquitin protein ligase E3A rat model of Angelman syndrome. *ENeuro* **8**:ENEURO.0345-20.2020. DOI: <https://doi.org/10.1523/ENEURO.0345-20.2020>, PMID: 33531368
- Buiting K**, Williams C, Horsthemke B. 2016. Angelman syndrome-insights into a rare neurogenetic disorder. *Nature Reviews Neurology* **12**:584–593. DOI: <https://doi.org/10.1038/nrneurol.2016.133>, PMID: 27615419
- Chen W**, Cai ZL, Chao ES, Chen H, Longley CM, Hao S, Chao HT, Kim JH, Messier JE, Zoghbi HY, Tang J, Swann JW, Xue M. 2020. STXBP1/munc18-1 haploinsufficiency impairs inhibition and mediates key neurological features of STXBP1 encephalopathy. *eLife* **9**:e48705. DOI: <https://doi.org/10.7554/eLife.48705>, PMID: 32073399
- Colas D**, Wagstaff J, Fort P, Salvert D, Sarda N. 2005. Sleep disturbances in UBE3A maternal-deficient mice modeling Angelman syndrome. *Neurobiology of Disease* **20**:471–478. DOI: <https://doi.org/10.1016/j.nbd.2005.04.003>, PMID: 15921919
- Copping NA**, McTighe SM, Fink KD, Silverman JL. 2021. Emerging gene and small molecule therapies for the neurodevelopmental disorder Angelman syndrome. *Neurotherapeutics* **18**:1535–1547. DOI: <https://doi.org/10.1007/s13311-021-01082-x>, PMID: 34528170
- Copping NA**, Silverman JL. 2021. Abnormal electrophysiological phenotypes and sleep deficits in a mouse model of angelman syndrome. *Molecular Autism* **12**:9. DOI: <https://doi.org/10.1186/s13229-021-00416-y>, PMID: 33549123
- Daily JL**, Nash K, Jinwal U, Golde T, Rogers J, Peters MM, Burdine RD, Dickey C, Banko JL, Weeber EJ. 2011. Adeno-associated virus-mediated rescue of the cognitive defects in a mouse model for angelman syndrome. *PLOS ONE* **6**:e27221. DOI: <https://doi.org/10.1371/journal.pone.0027221>, PMID: 22174738
- Dindot SV**, Antalffy BA, Bhattacharjee MB, Beaudet AL. 2008. The Angelman syndrome ubiquitin ligase localizes to the synapse and nucleus, and maternal deficiency results in abnormal dendritic spine morphology. *Human Molecular Genetics* **17**:111–118. DOI: <https://doi.org/10.1093/hmg/ddm288>, PMID: 17940072
- Ehlen JC**, Jones KA, Pinckney L, Gray CL, Burette S, Weinberg RJ, Evans JA, Brager AJ, Zylka MJ, Paul KN, Philpot BD, DeBruyne JP. 2015. Maternal *Ube3a* loss disrupts sleep homeostasis but leaves circadian rhythmicity largely intact. *The Journal of Neuroscience* **35**:13587–13598. DOI: <https://doi.org/10.1523/JNEUROSCI.2194-15.2015>, PMID: 26446213
- Elgersma Y**, Sonzogni M. 2021. *Ube3a* reinstatement as a disease-modifying therapy for Angelman syndrome. *Developmental Medicine and Child Neurology* **63**:802–807. DOI: <https://doi.org/10.1111/dmcn.14831>, PMID: 33543479
- Frohlich J**, Miller MT, Bird LM, Garces P, Purtell H, Hoener MC, Philpot BD, Sidorov MS, Tan WH, Hernandez MC, Rotenberg A, Jeste SS, Krishnan M, Khwaja O, Hipp JF. 2019. Electrophysiological phenotype in Angelman

- syndrome differs between genotypes. *Biological Psychiatry* **85**:752–759. DOI: <https://doi.org/10.1016/j.biopsych.2019.01.008>, PMID: 30826071
- Grier MD**, Carson RP, Lagrange AH. 2015. Toward a broader view of Ube3a in a mouse model of Angelman syndrome: expression in brain, spinal cord, sciatic nerve and glial cells. *PLOS ONE* **10**:e0124649. DOI: <https://doi.org/10.1371/journal.pone.0124649>, PMID: 25894543
- Gu B**, Carstens KE, Judson MC, Dalton KA, Rougié M, Clark EP, Dudek SM, Philpot BD. 2019. Ube3A reinstatement mitigates epileptogenesis in Angelman syndrome model mice. *The Journal of Clinical Investigation* **129**:163–168. DOI: <https://doi.org/10.1172/JCI120816>, PMID: 30352049
- Harlalka GV**, Baple EL, Cross H, Kühnle S, Cubillos-Rojas M, Matentzoglu K, Patton MA, Wagner K, Coblenz R, Ford DL, Mackay DJG, Chioza BA, Scheffner M, Rosa JL, Crosby AH. 2013. Mutation of HERC2 causes developmental delay with angelman-like features. *Journal of Medical Genetics* **50**:65–73. DOI: <https://doi.org/10.1136/jmedgenet-2012-101367>, PMID: 23243086
- Hipp JF**, Frohlich J, Keute M, Tan WH, Bird LM. 2021. Electrophysiological abnormalities in Angelman syndrome correlate with symptom severity. *Biological Psychiatry Global Open Science* **1**:201–209. DOI: <https://doi.org/10.1016/j.bpsgos.2021.05.003>, PMID: 34841387
- Huang HS**, Allen JA, Mabb AM, King IF, Miriyala J, Taylor-Blake B, Sciaky N, Dutton JW, Lee HM, Chen X, Jin J, Bridges AS, Zylka MJ, Roth BL, Philpot BD. 2011. Topoisomerase inhibitors unsilence the dormant allele of Ube3a in neurons. *Nature* **481**:185–189. DOI: <https://doi.org/10.1038/nature10726>, PMID: 22190039
- Huang HS**, Burns AJ, Nonneman RJ, Baker LK, Riddick NV, Nikolova VD, Riday TT, Yashiro K, Philpot BD, Moy SS. 2013. Behavioral deficits in an angelman syndrome model: effects of genetic background and age. *Behavioural Brain Research* **243**:79–90. DOI: <https://doi.org/10.1016/j.bbr.2012.12.052>, PMID: 23295389
- Jiang YH**, Armstrong D, Albrecht U, Atkins CM, Noebels JL, Eichele G, Sweatt JD, Beaudet AL. 1998. Mutation of the Angelman ubiquitin ligase in mice causes increased cytoplasmic p53 and deficits of contextual learning and long-term potentiation. *Neuron* **21**:799–811. DOI: [https://doi.org/10.1016/s0896-6273\(00\)80596-6](https://doi.org/10.1016/s0896-6273(00)80596-6), PMID: 9808466
- Jiang YH**, Pan Y, Zhu L, Landa L, Yoo J, Spencer C, Lorenzo I, Brilliant M, Noebels J, Beaudet AL. 2010. Altered ultrasonic vocalization and impaired learning and memory in angelman syndrome mouse model with a large maternal deletion from ube3a to gabrb3. *PLOS ONE* **5**:e12278. DOI: <https://doi.org/10.1371/journal.pone.0012278>, PMID: 20808828
- Judson MC**, Sosa-Pagan JO, Del Cid WA, Han JE, Philpot BD. 2014. Allelic specificity of Ube3a expression in the mouse brain during postnatal development. *The Journal of Comparative Neurology* **522**:1874–1896. DOI: <https://doi.org/10.1002/cne.23507>, PMID: 24254964
- Judson MC**, Wallace ML, Sidorov MS, Burette AC, Gu B, van Woerden GM, King IF, Han JE, Zylka MJ, Elgersma Y, Weinberg RJ, Philpot BD. 2016. GABAergic neuron-specific loss of ube3a causes angelman syndrome-like EEG abnormalities and enhances seizure susceptibility. *Neuron* **90**:56–69. DOI: <https://doi.org/10.1016/j.neuron.2016.02.040>, PMID: 27021170
- Judson MC**, Shyng C, Simon JM, Davis CR, Punt AM, Salmon MT, Miller NW, Ritola KD, Elgersma Y, Amaral DG, Gray SJ, Philpot BD. 2021. Dual-isoform hube3a gene transfer improves behavioral and seizure outcomes in angelman syndrome model mice. *JCI Insight* **6**:144712. DOI: <https://doi.org/10.1172/jci.insight.144712>
- Kaku HN**. 2022. Angelman. swh:1:rev:a8e5152b011de54a1d2b3ea468a07fe7e2345c5f. Software Heritage. <https://archive.softwareheritage.org/swh:1:dir:2d3231723e548bab4dba569ce4577cb998f0935;origin=https://github.com/heetkaku/angelman;visit=swh:1:snp:3a4d5dc43783ea112e7bf08de6980660b66ccfb;anchor=swh:1:rev:a8e5152b011de54a1d2b3ea468a07fe7e2345c5f>
- Kishino T**, Lalonde M, Wagstaff J. 1997. UBE3A/E6-AP mutations cause Angelman syndrome. *Nature Genetics* **15**:70–73. DOI: <https://doi.org/10.1038/ng0197-70>, PMID: 8988171
- Kühnle S**, Kogel U, Glockzin S, Marquardt A, Ciechanover A, Matentzoglu K, Scheffner M. 2011. Physical and functional interaction of the HECT ubiquitin-protein ligases E6AP and HERC2. *The Journal of Biological Chemistry* **286**:19410–19416. DOI: <https://doi.org/10.1074/jbc.M110.205211>, PMID: 21493713
- Mandel-Brehm C**, Salogiannis J, Dhamne SC, Rotenberg A, Greenberg ME. 2015. Seizure-like activity in a juvenile angelman syndrome mouse model is attenuated by reducing ARC expression. *PNAS* **112**:5129–5134. DOI: <https://doi.org/10.1073/pnas.1504809112>, PMID: 25848016
- Margolis SS**, Sell GL, Zbinden MA, Bird LM. 2015. Angelman syndrome. *Neurotherapeutics* **12**:641–650. DOI: <https://doi.org/10.1007/s13311-015-0361-y>, PMID: 26040994
- Markati T**, Duis J, Servais L. 2021. Therapies in preclinical and clinical development for Angelman syndrome. *Expert Opinion on Investigational Drugs* **30**:709–720. DOI: <https://doi.org/10.1080/13543784.2021.1939674>, PMID: 34112038
- Matsuura T**, Sutcliffe JS, Fang P, Galjaard RJ, Jiang YH, Benton CS, Rommens JM, Beaudet AL. 1997. De novo truncating mutations in E6-AP ubiquitin-protein ligase gene (Ube3a) in Angelman syndrome. *Nature Genetics* **15**:74–77. DOI: <https://doi.org/10.1038/ng0197-74>, PMID: 8988172
- Meng L**, Person RE, Beaudet AL. 2012. Ube3a-ATS is an atypical RNA polymerase II transcript that represses the paternal expression of Ube3a. *Human Molecular Genetics* **21**:3001–3012. DOI: <https://doi.org/10.1093/hmg/ddr130>, PMID: 22493002
- Meng L**, Person RE, Huang W, Zhu PJ, Costa-Mattioli M, Beaudet AL. 2013. Truncation of UBE3A-ATS unsilences paternal UBE3A and ameliorates behavioral defects in the angelman syndrome mouse model. *PLOS Genetics* **9**:e1004039. DOI: <https://doi.org/10.1371/journal.pgen.1004039>, PMID: 24385930

- Meng L**, Ward AJ, Chun S, Bennett CF, Beaudet AL, Rigo F. 2015. Towards a therapy for Angelman syndrome by targeting a long non-coding RNA. *Nature* **518**:409–412. DOI: <https://doi.org/10.1038/nature13975>, PMID: 25470045
- Miano S**, Bruni O, Leuzzi V, Elia M, Verrillo E, Ferri R. 2004. Sleep polygraphy in Angelman syndrome. *Clinical Neurophysiology* **115**:938–945. DOI: <https://doi.org/10.1016/j.clinph.2003.11.004>, PMID: 15003776
- Miano S**, Bruni O, Elia M, Musumeci SA, Verrillo E, Ferri R. 2005. Sleep breathing and periodic leg movement pattern in Angelman syndrome: a polysomnographic study. *Clinical Neurophysiology* **116**:2685–2692. DOI: <https://doi.org/10.1016/j.clinph.2005.08.005>, PMID: 16213786
- Miao S**, Chen R, Ye J, Tan G-H, Li S, Zhang J, Jiang Y, Xiong Z-Q. 2013. The Angelman syndrome protein Ube3a is required for polarized dendrite morphogenesis in pyramidal neurons. *The Journal of Neuroscience* **33**:327–333. DOI: <https://doi.org/10.1523/JNEUROSCI.2509-12.2013>, PMID: 23283345
- Miladinović Đ**, Muheim C, Bauer S, Spinnler A, Noain D, Bandarabadi M, Gallusser B, Krummenacher G, Baumann C, Adamantidis A, Brown SA, Buhmann JM. 2019. Spindle: end-to-end learning from EEG/EMG to extrapolate animal sleep scoring across experimental settings, labs and species. *PLOS Computational Biology* **15**:e1006968. DOI: <https://doi.org/10.1371/journal.pcbi.1006968>, PMID: 30998681
- Milazzo C**, Mientjes EJ, Wallaard I, Rasmussen SV, Erichsen KD, Kakunuri T, van der Sman ASE, Kremer T, Miller MT, Hoener MC, Elgersma Y. 2021. Antisense oligonucleotide treatment rescues ube3a expression and multiple phenotypes of an angelman syndrome mouse model. *JCI Insight* **6**:e145991. DOI: <https://doi.org/10.1172/jci.insight.145991>, PMID: 34369389
- Miura K**, Kishino T, Li E, Webber H, Dikkes P, Holmes GL, Wagstaff J. 2002. Neurobehavioral and electroencephalographic abnormalities in ube3a maternal-deficient mice. *Neurobiology of Disease* **9**:149–159. DOI: <https://doi.org/10.1006/nbdi.2001.0463>, PMID: 11895368
- Møller RS**, Wuttke TV, Helbig I, Marini C, Johannesen KM, Brilstra EH, Vaher U, Borggraefe I, Talvik I, Talvik T, Kluger G, Francois LL, Lesca G, de Bellescize J, Blichfeldt S, Chatron N, Holert N, Jacobs J, Swinkels M, Betzler C, et al. 2017. Mutations in GABRB3: from febrile seizures to epileptic encephalopathies. *Neurology* **88**:483–492. DOI: <https://doi.org/10.1212/WNL.0000000000003565>, PMID: 28053010
- Ostrowski LM**, Spencer ER, Bird LM, Thibert R, Komorowski RW, Kramer MA, Chu CJ. 2021. Delta power robustly predicts cognitive function in Angelman syndrome. *Annals of Clinical and Translational Neurology* **8**:1433–1445. DOI: <https://doi.org/10.1002/acn3.51385>, PMID: 34047077
- Puffenberger EG**, Jinks RN, Wang H, Xin B, Fiorentini C, Sherman EA, Degrazio D, Shaw C, Sougnez C, Cibulskis K, Gabriel S, Kelley RL, Morton DH, Strauss KA. 2012. A homozygous missense mutation in HERC2 associated with global developmental delay and autism spectrum disorder. *Human Mutation* **33**:1639–1646. DOI: <https://doi.org/10.1002/humu.22237>, PMID: 23065719
- Rotaru DC**, van Woerden GM, Wallaard I, Elgersma Y. 2018. Adult ube3a gene reinstatement restores the electrophysiological deficits of prefrontal cortex layer 5 neurons in a mouse model of angelman syndrome. *The Journal of Neuroscience* **38**:8011–8030. DOI: <https://doi.org/10.1523/JNEUROSCI.0083-18.2018>, PMID: 30082419
- Rotaru DC**, Mientjes EJ, Elgersma Y. 2020. Angelman syndrome: from mouse models to therapy. *Neuroscience* **445**:172–189. DOI: <https://doi.org/10.1016/j.neuroscience.2020.02.017>, PMID: 32088294
- Rougeulle C**, Glatt H, Lalonde M. 1997. The Angelman syndrome candidate gene, UBE3A/E6-AP, is imprinted in brain. *Nature Genetics* **17**:14–15. DOI: <https://doi.org/10.1038/ng0997-14>, PMID: 9288088
- Schmid RS**, Deng X, Panikker P, Msacky I, Breton C, Wilson JM. 2021. Crispr/Cas9 directed to the Ube3a antisense transcript improves Angelman syndrome phenotype in mice. *The Journal of Clinical Investigation* **131**:e142574. DOI: <https://doi.org/10.1172/JCI142574>, PMID: 33411694
- Shi SQ**, Mahoney CE, Houdek P, Zhao W, Anderson MP, Zhuo X, Beaudet A, Sumova A, Scammell TE, Johnson CH. 2022. Circadian rhythms and sleep are dependent upon expression levels of key ubiquitin ligase Ube3a. *Frontiers in Behavioral Neuroscience* **16**:837523. DOI: <https://doi.org/10.3389/fnbeh.2022.837523>, PMID: 35401134
- Sidorov MS**, Deck GM, Dolatshahi M, Thibert RL, Bird LM, Chu CJ, Philpot BD. 2017. Delta rhythmicity is a reliable EEG biomarker in angelman syndrome: a parallel mouse and human analysis. *Journal of Neurodevelopmental Disorders* **9**:17. DOI: <https://doi.org/10.1186/s11689-017-9195-8>, PMID: 28503211
- Silva-Santos S**, van Woerden GM, Bruinsma CF, Mientjes E, Jolfaei MA, Distel B, Kushner SA, Elgersma Y. 2015. Ube3A reinstatement identifies distinct developmental windows in a murine Angelman syndrome model. *The Journal of Clinical Investigation* **125**:2069–2076. DOI: <https://doi.org/10.1172/JCI80554>, PMID: 25866966
- Sonzogni M**, Wallaard I, Santos SS, Kingma J, du Mee D, van Woerden GM, Elgersma Y. 2018. A behavioral test battery for mouse models of angelman syndrome: A powerful tool for testing drugs and novel ube3a mutants. *Molecular Autism* **9**:47. DOI: <https://doi.org/10.1186/s13229-018-0231-7>, PMID: 30220990
- Sonzogni M**, Zhai P, Mientjes EJ, van Woerden GM, Elgersma Y. 2020. Assessing the requirements of prenatal ube3a expression for rescue of behavioral phenotypes in a mouse model for angelman syndrome. *Molecular Autism* **11**:70. DOI: <https://doi.org/10.1186/s13229-020-00376-9>, PMID: 32948244
- Spencer ER**, Shi W, Komorowski RW, Gilbert JP, Ostrowski LM, Bird LM, Thibert R, Bao C, Molloy F, Calhoun M, Koerala S, Jafar-Nejad P, Rigo F, Kramer MA, Chu CJ. 2022. Longitudinal EEG model detects antisense oligonucleotide treatment effect and increased Ube3a in Angelman syndrome. *Brain Communications* **4**:fcac106. DOI: <https://doi.org/10.1093/braincomms/fcac106>, PMID: 35611307
- Spruyt K**, Braam W, Curfs LM. 2018. Sleep in Angelman syndrome: a review of evidence. *Sleep Medicine Reviews* **37**:69–84. DOI: <https://doi.org/10.1016/j.smrv.2017.01.002>, PMID: 28784434

- Swayze EE**, Siwkowski AM, Wancewicz EV, Migawa MT, Wyrzykiewicz TK, Hung G, Monia BP, Bennett CF. 2007. Antisense oligonucleotides containing locked nucleic acid improve potency but cause significant hepatotoxicity in animals. *Nucleic Acids Research* **35**:687–700. DOI: <https://doi.org/10.1093/nar/gkl1071>, PMID: 17182632
- Weeber EJ**, Jiang YH, Elgersma Y, Varga AW, Carrasquillo Y, Brown SE, Christian JM, Mirnikjoo B, Silva A, Beaudet AL, Sweatt JD. 2003. Derangements of hippocampal calcium/calmodulin-dependent protein kinase II in a mouse model for angelman mental retardation syndrome. *The Journal of Neuroscience* **23**:2634–2644. DOI: <https://doi.org/10.1523/JNEUROSCI.23-07-02634.2003>, PMID: 12684449
- Welch P.** 1967. The use of fast fourier transform for the estimation of power spectra: A method based on time averaging over short, modified periodograms. *IEEE Transactions on Audio and Electroacoustics* **15**:70–73. DOI: <https://doi.org/10.1109/TAU.1967.1161901>
- Willgoss T**, Cassater D, Connor S, Krishnan ML, Miller MT, Dias-Barbosa C, Phillips D, McCormack J, Bird LM, Burdine RD, Claridge S, Bichell TJ. 2021. Measuring what matters to individuals with Angelman syndrome and their families: development of a patient-centered disease concept model. *Child Psychiatry and Human Development* **52**:654–668. DOI: <https://doi.org/10.1007/s10578-020-01051-z>, PMID: 32880036
- Williams CA**, Beaudet AL, Clayton-Smith J, Knoll JH, Kyllerman M, Laan LA, Magenis RE, Moncla A, Schinzel AA, Summers JA, Wagstaff J. 2006. Angelman syndrome 2005: updated consensus for diagnostic criteria. *American Journal of Medical Genetics. Part A* **140**:413–418. DOI: <https://doi.org/10.1002/ajmg.a.31074>, PMID: 16470747
- Wolter JM**, Mao H, Fragola G, Simon JM, Krantz JL, Bazick HO, Oztemiz B, Stein JL, Zylka MJ. 2020. Cas9 gene therapy for Angelman syndrome traps ube3a-ATS long non-coding RNA. *Nature* **587**:281–284. DOI: <https://doi.org/10.1038/s41586-020-2835-2>, PMID: 33087932
- Yang X.** 2020. Towards an understanding of Angelman syndrome in mice studies. *Journal of Neuroscience Research* **98**:1162–1173. DOI: <https://doi.org/10.1002/jnr.24576>, PMID: 31867793
- Yashiro K**, Riday TT, Condon KH, Roberts AC, Bernardo DR, Prakash R, Weinberg RJ, Ehlers MD, Philpot BD. 2009. Ube3a is required for experience-dependent maturation of the neocortex. *Nature Neuroscience* **12**:777–783. DOI: <https://doi.org/10.1038/nn.2327>, PMID: 19430469
- Zeiss CJ.** 2021. Comparative milestones in rodent and human postnatal central nervous system development. *Toxicologic Pathology* **49**:1368–1373. DOI: <https://doi.org/10.1177/01926233211046933>, PMID: 34569375